KfK 3161
April 1981

Bénard Convection in Gaps and Cavities

U. Müller
Institut für Reaktorbauelemente

Kernforschungszentrum Karlsruhe

KERNFORSCHUNGSZENTRUM KARLSRUHE
Institut für Reaktorbauelemente

KfK 3161

Bénard Convection in Gaps and Cavities

U. Müller

Kernforschungszentrum Karlsruhe GmbH, Karlsruhe

Kernforschungszentrum Karlsruhe GmbH
ISSN 0303-4003

Bénard Convection in Gaps and Cavities

Summary

The article contains two parts. In the first part a condensed review of the most striking phenomena in Bénard convection in laterally confined fluid layers is given. In the second part recent experimental and theoretical work on Bénard convection in gaps is presented and analysed.

Bénard-Konvektion in Spalten und Hohlräumen

Zusammenfassung

Der Bericht enthält eine zusammenfassende Darstellung der wesentlichen Einflüsse seitlicher Berandungen auf die freie Konvektion in von unten beheizten Flüssigkeitsschichten. Besondere Berücksichtigung finden dabei neuere experimentelle und theoretische Arbeiten über die freie Konvektion in vertikalen Spalten.

Contents

1. Introduction

The study of Bénard Convection in containers of moderate size is stimulated mainly by two basically different areas of interest, namely, application in engineering technology and fundamental studies in laminar-turbulent transition.

Engineering technology requires better understanding of gravity induced heat and mass transport for the design of e. g. thermosiphons /1/ solar collectors /2, 34, 35, 36/ heat storage systems, crystal growth reactors /3, 10, 57, 58/ safety precaution systems in nuclear technology. The objective of such investigations may be enhancement, suppression or control of the transport process.

Recently new ideas related to the transition from laminar to turbulent flow /4,5,6/ have fostered precision experiments on Bénard convection in small boxes. In these experiments Laser-Doppler anemometry, interferometry, precision temperature probes and/or cryotechnique have been employed /7,8,9/. These techniques generally necessitate small test volumes of regular geometry. The interpretation of the experimental findings naturally requires precise knowledge of the side wall effects.

2. Problem

Experimentalists studying Bénard convection have early recognized, that the lateral walls of their test chambers influence or even determine the cellular pattern in the fluid layer /11,12/. Thus in cylindrical containers the generation of axisymmetric roll systems seemed to be favoured whereas in rectangular boxes a system of straight rolls parallel to the side walls were found.

A rigorous analytical treatment of the influence of the side walls even for the problem of onset of convection in containers (linearized problem) takes more effort compared to the case of infinite layers, as the separability of the variables in the linearized Oberbeck-Boussinesq equations (O.B.E. see /13/) is lost due to additional boundary conditions at the side walls.

For a realistic description of confined heated flow a kinematic 'no slip' condition must hold for all rigid boundaries. The thermal conditions at the boundaries may be perfectly conducting walls only or in part adiabatic walls or even walls of finite thermal conductivity. As an example the problem describing the onset of convection in a rectangular box with isothermal horizontal and adiabatic side walls is formulated below, the geometry is sketched in fig. 1 (for more general outlines see /14, 15/).

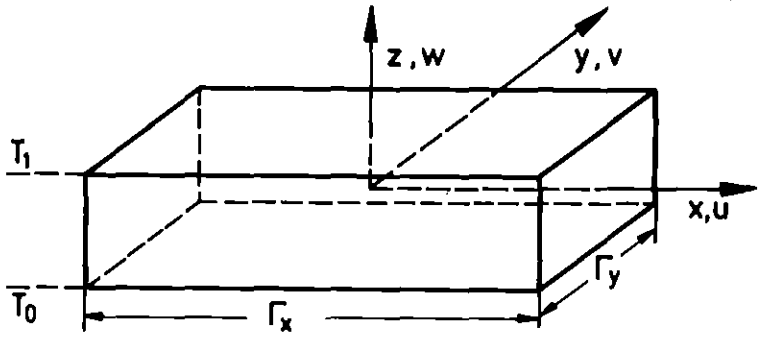

Figure 1: Sketch of rectangular cavity.

O.B.E.: $Pr^{-1}\,(\partial_t \underset{\sim}{v} + (\underset{\sim}{v}\cdot\nabla)\underset{\sim}{v}) = -\nabla\pi + \nu\Delta\underset{\sim}{v} + Ra\theta e_3$,

$\partial_t\theta + (\underset{\sim}{v}\cdot\nabla)\theta - w = \Delta\theta$,

$\underset{\sim}{v} = 0$.

boundary conditions

$(x,y,z) = (\pm\frac{1}{2}\Gamma_{x_1} \pm \frac{1}{2}\Gamma_{y_1} \pm \frac{1}{2})$ 'no slip' walls,

$\partial_x\theta = 0,\ x = \pm\frac{1}{2}\Gamma_x$

$\partial_y\theta = 0,\ y = \pm\frac{1}{2}\Gamma_y$ adiabatic side walls,

$\theta = 0,\ z = \pm\frac{1}{2}$ isothermal horizontal walls,

where

$$Ra = \frac{\alpha\cdot g\cdot(T_o - T_1)\cdot h^3}{\kappa\cdot\nu}$$ Rayleigh number,

$Pr = \nu/\kappa$ Prandtl number,

Γ_x , Γ_y aspect ratio

$\Delta: = \partial^2_{xx} + \partial^2_{yy} + \partial^2_{zz}$

$\underset{\sim}{v} = (u, v, w)$ velocities,

θ perturbation temperature.

e_3 unit vector in z-direction

In order to maintain separability of the variables and thus benefit from a simpler mathematical problem theoreticans have often replaced 'no slip' conditions at the vertical or horizontal walls by slip conditions /15, 16, 17, 18 /. It is evident that for certain problems good approximations can be achieved by this assumption. This is for instance the case either for large ('slip' side walls) or very small ('slip' horizontal walls) aspect ratios.

α - coefficient of thermal expansion; g - acceleration of gravity;
ν - kinematic viscosity; κ - coefficient of thermal diffusion;
h - layer height; $T_o - T_1$ - temperature difference across fluid layer.

3. Convection in Cavities

3.1 Onset of Convection and Flow Pattern

Side walls have generally a stabilizing effect on heat conducting horizontal fluid layers. The critical Rayleigh numbers defining the onset of convection are usually calculated by a Galerkin procedure taking into account the complete set of boundary conditions. Calculations have been performed for rectangular and cylindrical containers for isothermal and adiabatic side walls and for aspect ratios $\Gamma \leq 10$. The results from calculations have been confirmed by experiments for common geometries /19 - 31/.

The main results of these investigations can be summarized as follows:

- The critical Rayleigh numbers strongly increase for aspect ratios smaller than one and approach closely the critical value Ra_c = 1708 of infinite layers for aspect ratios of the order five.

- Adiabatic side walls result in lower critical Rayleigh numbers compared to isothermal side walls for the same aspect ratios.

- In rectangular boxes the axes of convection rolls are aligned parallel to the shorter side of the box (the degeneracy of the spacial orientation of the cellular patterns is raised by the viscous effects of the side walls except squares).

The first and the third effect can be seen from fig. 2, where together with caluclations the experimental verification is demonstrated /19, 20, 86/.

Recent experiments as well as more detailed three-dimensional analytical and numerical calculations have revealed that even at the threshold of convection the flow pattern in rectangular containers has a three-dimensional structure. A strong three-dimensionality of the velocity field is, however, limited to the corner regions /31-33/.

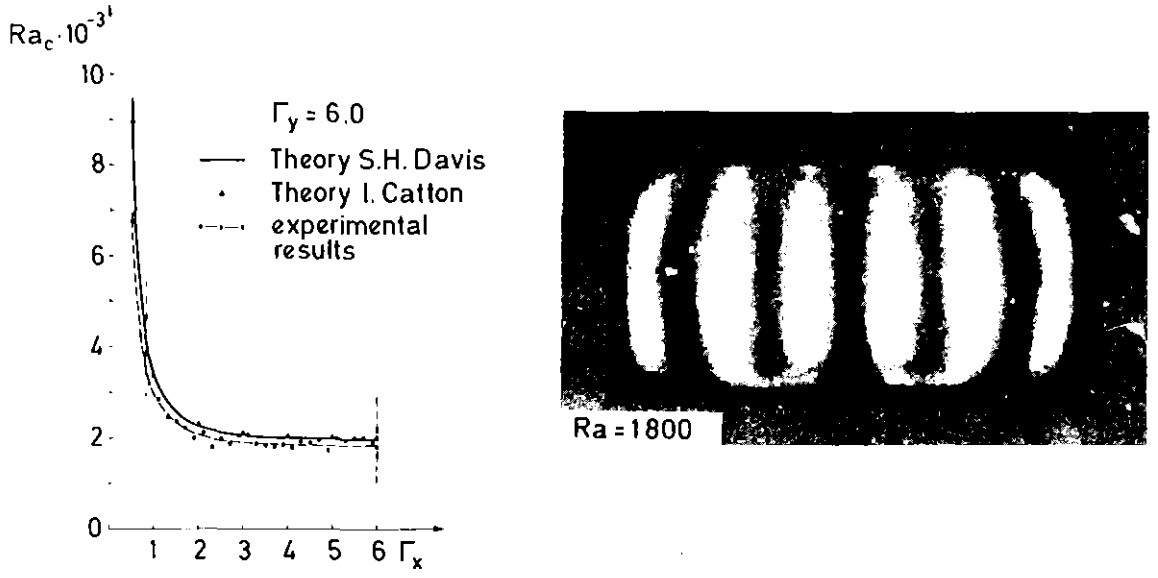

Figure 2: Critical Rayleigh numbers and flow pattern in a rectangular box. Aspect ratios for the critical Rayleigh numbers ($h_1 = \Gamma_x$, $h_2 = \Gamma_y$) $\Gamma_x = 6$, $0.6 < \Gamma_y < 6$, aspect ratio for flow pattern $\Gamma_x = 6$, $\Gamma_y = 3$.

The question of pattern at onset of convection in cylindrical containers is more subtle. Calculations show that for aspect ratios $\Gamma_r < 1$ an antisymmetric flow pattern occurs, whereas for aspect ratios $1 \lesssim \Gamma_r \lesssim 2$ an axisymmetric pattern is realized. For aspect ratios greater than two the calculations according to a linear stability theory predict axisymmetric and non-axisymmetric pattern depending on the thermal boundary conditions of the side walls and the aspect ratio. Indeed stable axisymmetric and non-axisymmetric flow pattern have been experimentally realized for aspect ratios larger than two /12, 25-28/. The non-axisymmetric pattern at small aspect ratios, where the side walls are supposed to influence the fluid flow most strongly, is surprising. A plausible explanation for the effect may be that a mismatch between an optimal torous roll diameter and the aspect ratio causes non-axisymmetry at moderate aspect ratios. A stability analysis for finite amplitude axisymmetric flows has shown that in certain cases depending on the Prandtl number, the aspect ratio and the

thermal boundary conditions axisymmetric pattern become unstable at slightly supercritical Rayleigh numbers /29, 30/. More research work is required before the questions of stability for axisymmetric modes can be answered conclusively.

3.2 Side Wall Induced Finite Amplitude Effects

It is generally accepted by theoreticans that the convective flow at slightly supercritical Rayleigh numbers can be reasonably well described by a perturbation analysis, in which the variables are developed in power series of the small quantity $\varepsilon = |(Ra-Ra_c)/Ra_c|^{1/2}$ (threshold measure). This procedure results in an ordinary non-linear differential equation in time for the amplitude V of the velocity (or temperature) and has the form: $\dot{V} = \alpha V + \beta V^3$ (α, β are parameters depending on the spacial structure of the flow). This equation is usually named Landau-Hopf equation and is assumed to be valid near the threshold of convection.

The range of validity of this amplitude equation has been investigated experimentally by performing measurements employing L.D.A. technique /37, 38/. According to these measurements the convection up to ten times the critical can be well described by only a few spacial modes in the power series.

As the measurements were taken in rectangular containers of moderate aspect ratio the influencing length, or in other words, the boundary layer thickness at the side walls was also quantified for different values ε. Within the scope of a generalized Landau-Hopf model for laterally confined layers /38/ the velocity maxima should vary in horizontal direction away from the wall according to $V(x) = V_0 \cdot \tanh \cdot (\frac{x}{\xi})$, V_0 being the velocity for $x \to \infty$. The predicted relation $\xi = 0.54 \cdot d \cdot \varepsilon^{-0.5}$ (d-layer height) was confirmed by measurements within an error bar of 6 %. The side wall influence can be seen from the schematically reproduced velocity measurements in fig. 3.

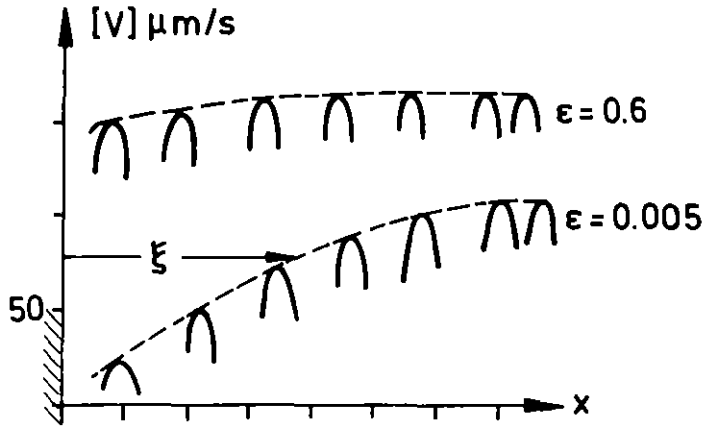

Figure 3: Influence length of lateral walls represented by velocity measurements within convection cells after /38/.

The conception of influence length has also been applied to subcritically induced convection /39/.

Subcritical cellular convection induced by wall properties (e.g. finite conductivity of side walls) has often been empirically employed by experimentalists to generate convection patterns of regular form (e.g. axisymmetric torous rolls) in containers of large aspect ratios /12, 26, 40, 41/. Using the experimentally verified correlation for the influence length the process can be controlled accordingly by regulating the quantity δ for the 'threshold distance' slowly enough in time.

An analytical model, which describes the transition from sub- to transcritical convection, for wall induced Bénard convection has been suggested based on the assumption, that the side walls have a finite but small heat conductivity /42-46/. Though all the calculations have been carried out for the physically unrealistic case of free lower and upper but rigid lateral surfaces the results apply qualitatively. A schematic graph of amplitude versus aspect ratio is given in fig. 4. The amplitude increases with increasing Rayleigh numbers from zero on and approaches smoothly the branch of the convection solution of an ideal O.B. system. The mathematical consequence of the thermal imperfection of the side wall is occasionally named 'imperfect bifurcation' /47/.

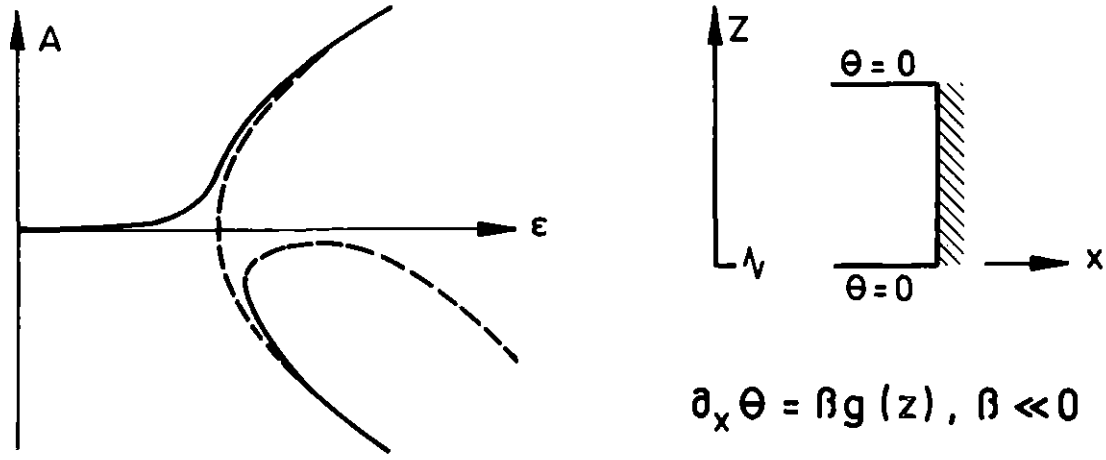

Figure 4: Smooth transition from rest to finite amplitude convection (solid line) in contrast to sharp transition (dashed line) after /46/.

From heat transfer measurements through convecting layers the smooth transition from the conductive to the convective state can often be well recognized from the Nusselt-Rayleigh number graph /26, 41 / (other than imperfections due to finite heat conductivity of the side walls may, however, lead to the same effect /42, 48/).

3.3 Supercritical Steady and Unsteady Convection

It has been regularly observed by experimentalists /49, 50/ that the cell diameter in cellular convection increases when the Rayleigh number is increased. In containers of large aspect ratio the adjustment process of the cell system is smooth, as due to pattern imperfections some convection rolls ending within the fluid layer are queesed off giving space to the others /85/. A similar continuous process is also realized in case of axisymmetric torous rolls, where the centre rolls vanish continuously one after the other /12, 26, 40/.

A system of parallel two-dimensional rolls in a rectangular cavity shows a different behaviour. As the roll system is fenced in by the side wall the increase (or decrease) of the roll diameter with increasing Rayleigh numbers proceeds quantized, that is after

periods in which no change in the number of rolls occurs when increasing the Rayleigh numbers one of the two outer rolls disappears in a 'snap through' process /53, 55, 56/. In the corresponding range of Rayleigh numbers the process shows hysteresis character. In the vicinity of the 'snap through' Rayleigh number the system is metastable and sensitive to any sort of perturbations. Intermittent time dependent events like fluctuations in the position of cell boundaries are observed to be repeatedly amplified and damped out. This sensitivity of the flow pattern is probably due to the mismatch between natural wave length for the convection rolls and the aspect ratio of the container. The degree of spacial symmetry characterized by an even or odd number of cells in the rectangular space influences in addition the stability of the roll system against spacial three-dimensional disturbances and/or fluctuations /31, 55/.

A great many of recent studies of unsteady thermal convection in small cavities are aimed mainly at supporting new models concerning the transition from laminar to turbulent flow /4-6/.
In these experiments local probes like L.D. instrumentation for velocity or thermocouples (thermistors) for temperature measurements were employed. By means of Fourier spectra of the signals the temporal structure of the flow is commonly analysed. Without giving details of the various studies the following characteristic features of the time dependent convective flow has been deduced from the spectra.

In cylindrical or rectangular cavities of small aspect ratio ($\Gamma \lesssim 4$) the unsteady convection starts in form of a time periodic motion (line spectrum of harmonics). Increasing the Rayleigh number the periodic flow is replaced by quasiperiodic motions (line spectra defining two frequencies). Increasing the Rayleigh number even more may render the flow periodic again (phase locking of the two frequencies, biperiodic flow).

Finally the flow produces stochastic signals and the spectra contain broad band noise indicating nonperiodic behaviour. The transition from periodic flow to 'turbulent flow' may also proceed via several successive subharmonic bifurcation /55, 59/.

For cavities of intermediate and large aspect ratios ($\Gamma \gtrsim 4$) the flow produces stochastic signals immediately at the threshold from steady to unsteady flow /60, 61, 57/.

3.4 Statements and Conclusions

The investigations on convective flow in containers of small and moderate aspect ratios have left open several questions.

The stability of steady state finite amplitude convection in cavities and its dependency on the aspect ratios, the Prandtl number and the Rayleigh number is insufficiently understood.

It is unclear to what extend the aspect ratios of the containers and their interference with other groups influence the transition to oscillatory and turbulent convective flow.

Although the local probe signal analysis applied to the Bénard problem in boxes has revealed a set of new phenomena, such investigations still have major shortcomings.

One of the most severe shortcomings is, that often the spacial structure of the convective flow in the various test chambers was insufficiently known during the experiment performance.

For a reasonable assessment of turbulence in a fluid flow, especially the detection of coherent structures, a simultaneous analysis of the spacial and the temporal structures of the flow is indispensable.

4. Convection in Gaps

4.1 General Remarks

Experimental and theoretical investigations have been carried out on Bénard convection in vertical gaps, so called Hele-Shaw cells, under aspects as outlined in chapter 3.4. A gap geometry was chosen, in order to keep the number of geometrical parameters as low as possible.

Holographic interferometry was employed for visualizing the spacial structure and thermocouples were used as local probes to record the temperature history. In addition numerical calculations have been performed in order to support explanations for the observed phenomena.

Similar, however less comprehensive investigations on Bénard convection in gaps have been reported by /63, 64/.

Free convection in Hele Shaw cells has been occasionally used by theoreticans and experimentalists to simulate gravity induced convective flows in porous media /62, 73-78/. This can be done because in both systems the specific fluxes are linearly correlated to pressure differences. The correlation is known as Darcy's law:

$$q = - \frac{k}{\mu} (\nabla p + \rho \underset{\sim}{g})$$

with q - flux vector, μ - dynamic viscosity, ρ - density, ∇p - pressure gradient, $\underset{\sim}{g}$ - acceleration of gravity vector and k - the permeability /79/. The permeability for the Hele Shaw cell can be derived as $k = d^3/12\ Y$, d-gap width of cell, Y-total thickness of cell (gap width plus two times the sidewall thickness) /80/.

The hydraulic analogy between a Hele Shaw cell and a porous medium is rigorous. However, in the case when temperatures act on the liquid solid system the thermal interaction between liquid and solid is difficult to model. Therefore usually averaging of thermal properties of the system is employed in order to obtain mathematically treatable models.

4.2 The Hele-Shaw Cell of Large Aspect Ratio

4.21 Onset of Convection

It has been discussed, whether the onset of convection in Hele-Shaw cells can be described uniformly by one properly defined Rayleigh number /80/. Such a Rayleigh number was given as

$$Ra = \alpha g \Delta T k h \cdot (\nu \kappa_m)^{-1}$$

with h - height of the cell, k - the permeability, ΔT - temperature difference between bottom and top, κ_m - average thermal diffusivity of fluid and solid walls.

Recent convection experiments, in Hele-Shaw cells constructed with side walls of different thermal properties (crystal glass or plexiglass) have shown that the onset of convection depends considerably on the gap and side wall thickness as well as on the heat conductivities of the liquid and solid phases /56/. However, the experimental findings are bounded by the physically ideal, mathematically rigorous cases of either perfectly conducting or perfectly insulating side walls /18/. The theory predicts in these cases that the critical Rayleigh numbers in the definition for infinite layers $Ra = \alpha g \Delta T h^3 (\nu \kappa)^{-1}$ varies as $Ra \sim A^2$ or $Ra \sim A^4$ for insulating or perfectly conducting side walls respectively, where A defines the aspect ratio (gap height over gap width). The experimental and theoretical results are summarized in fig. 5. These results are not surprising, as it is known from other investigations that reducing the heat conductivity of the boundaries decreases the critical Rayleigh number /81/. It demonstrates more over that the porous media approximation for the Rayleigh number in a Hele-Shaw cell is only suitable for certain combinations of geometries and thermal properties of the confining walls.

4.22 The Stability of Steady Convection in Hele-Shaw Cells

A question of fundamental and applied interest /70/ is the stability of steady state, two-dimensional convection in Hele-Shaw

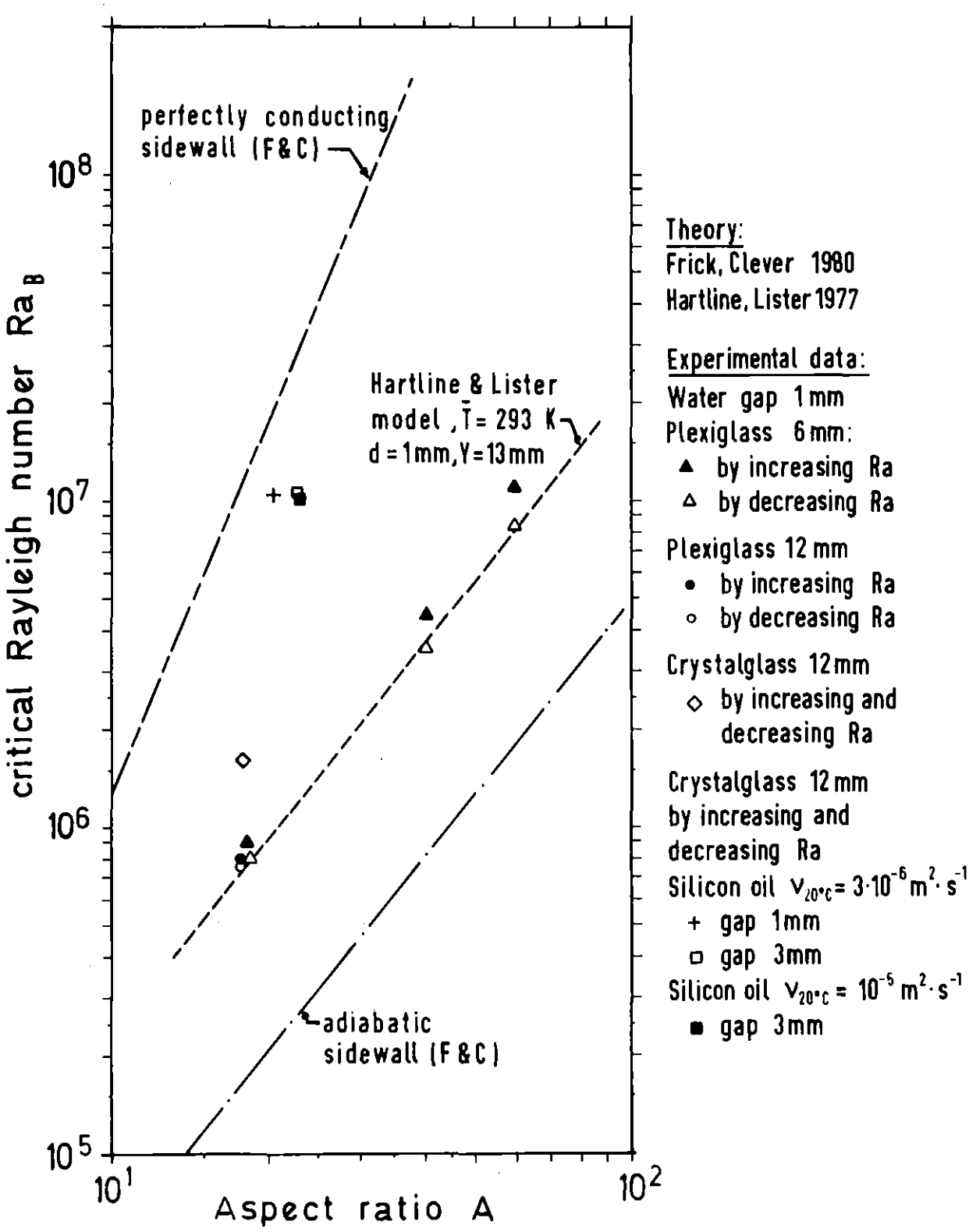

Figure 5: Critical Rayleigh numbers for Hele-Shaw cells of different height to depth ratios h/d and different side wall materials. For comparison see theoretical results of /18/ and /80/.

cells. This question has been investigated both theoretically and experimentally /56, 68, 69/. The theoretical results /69, 68/ have been obtained by a stability analysis of the steady state nonlinear solutions of the Boussinesq equations by employing a Galerkin procedure. For scrutinizing the theoretical results experiments were performed in a Hele-Shaw cell having plexiglass side walls and water as the test fluid. The theoretical and experimental results are compiled in fig. 6. In the graph the different states are characterized by the ratio of the actual to the critical Rayleigh number Ra/Ra_c and the ratio of the actual to the critical wave number α/α_c. The theoretical boundaries of neutral, Eckhaus and oscillatory instability are marked by dash-dotted, solid and dashed lines respectively. According to theory stable steady two-dimensional convection should only occur within the area confined by the solid and the dashed line.

The question is, to what extend do the experimental results confirm these prediction?

In the first test series (solid dots left row in fig. 6) steady states of convection with a frozen wave length close to critical could be achieved successively by quasi steady increasing the temperature difference in certain intervalls. Transition to unsteady oscillatory convection occurred at about ten times the critical Rayleigh number. This is in good agreement with the predictions of the theory, according to which oscillations should be observed at supercritical Rayleigh number $Ra/Ra_c \approx 10$; /68, 69/.

In a second "sudden start" experiment (solid dots right side in fig. 6) the stability of steady state convection against perturbations of oscillatory type was explored for supercritical wave numbers and very high supercritical Rayleigh numbers. Starting at a Rayleigh number ratio $Ra/Ra_c \approx 9.5$ unsteady oscillatory convection occurred first at $Ra/Ra_c \approx 16$ after the temperature difference had been increased in a quasi steady manner in certain time intervals. The agreement between the experimental and theoretical findings are considered as satisfying although the experimental values lie below the extrapolation of the theoretical curve for oscillatory instability. In this context it should be realized

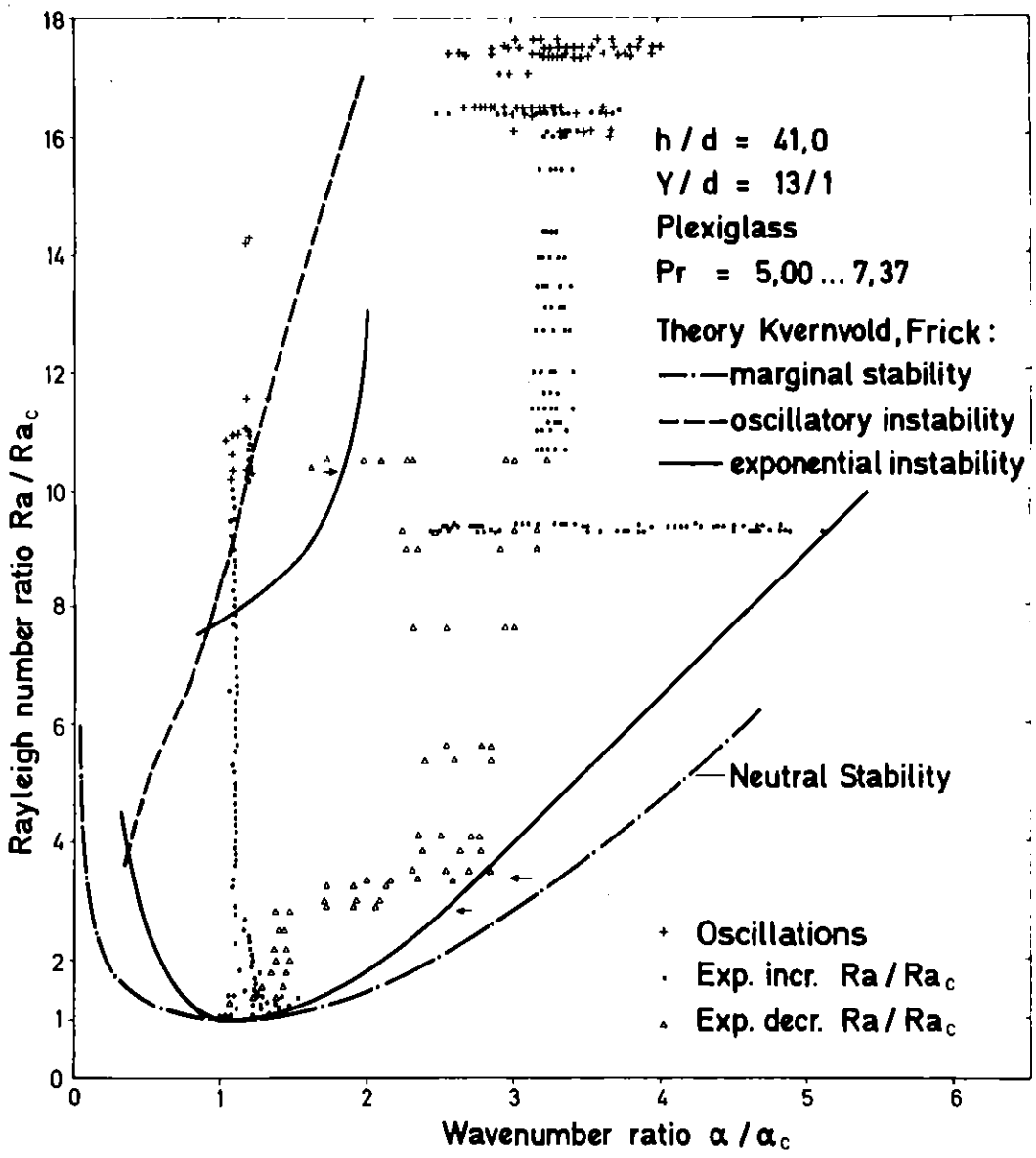

Figure 6: Stability map of tow-dimensional convective flow in a Hele-Shaw cell in reduced variables Ra/Ra_c, α/α_c, Ra_c - critical Rayleigh number and α_c - critical wave number at onset of convection. Experiments were performed in a Hele-Shaw cell with plexi glass walls, water as a test fluid and aspect ratios h/d = 41, h/b = 0.095. Lines correspond to theoretical results /68, 69/ dots experimental results /56/.

that on one side for the calculations simplifying assumptions concerning the symmetry of the flow were made for saving computing time and on the other side the high temperature differences ($\Delta T \sim 10$ K) across the Hele-Shaw cell may have caused experimental imperfections.

An initial steady state at 10.5 Ra/Ra_c can be established at the beginning of a third test series (white triangles in fig. 6) by acting on the fluid layer in the gap by a certain empirical heating history. This initial state was characterized by a set of convection cells of different wave length. When the Rayleigh number is reduced by reducing the temperature difference, the cell sizes became adapted to a mean value of $\alpha/\alpha_c \sim 2.5$. As the Rayleigh and wave numbers approache values corresponding to the bounding curve of Eckhaus instability (see fig. 6) the wave number of the cells is reduced when the Rayleigh number was decreased furtheron. This indicates that Eckhaus instability indeed limits the stable range of two-dimensional steady convection. The decrease in the wave number (or the increase in cell size respectively) occurred in an unsteady "snap through" process eliminating one cell from the finite length Hele-Shaw system in one step. This process was repeated when the Rayleigh number was further reduced. Three steps were observed during the experiment. The experiment thus validates the stability theory of /69/.

The investigations have thus shown, that as far as the stability of the steady state two-dimensional flow in Hele-Shaw cells is concerned theory and experiment are in good agreement.

4.23 The Spacial and Temporal Structure of Unsteady Convection in Hele-Shaw Cells

Employing real time holographic interferometry origins of unsteadyness in the flow have been localized. The main source for generating unsteady flow can be recognized from fig. 7, in which a series of interferograms photographed in succeeding time intervals is shown. In the temperature boundary layer near the lower hori-

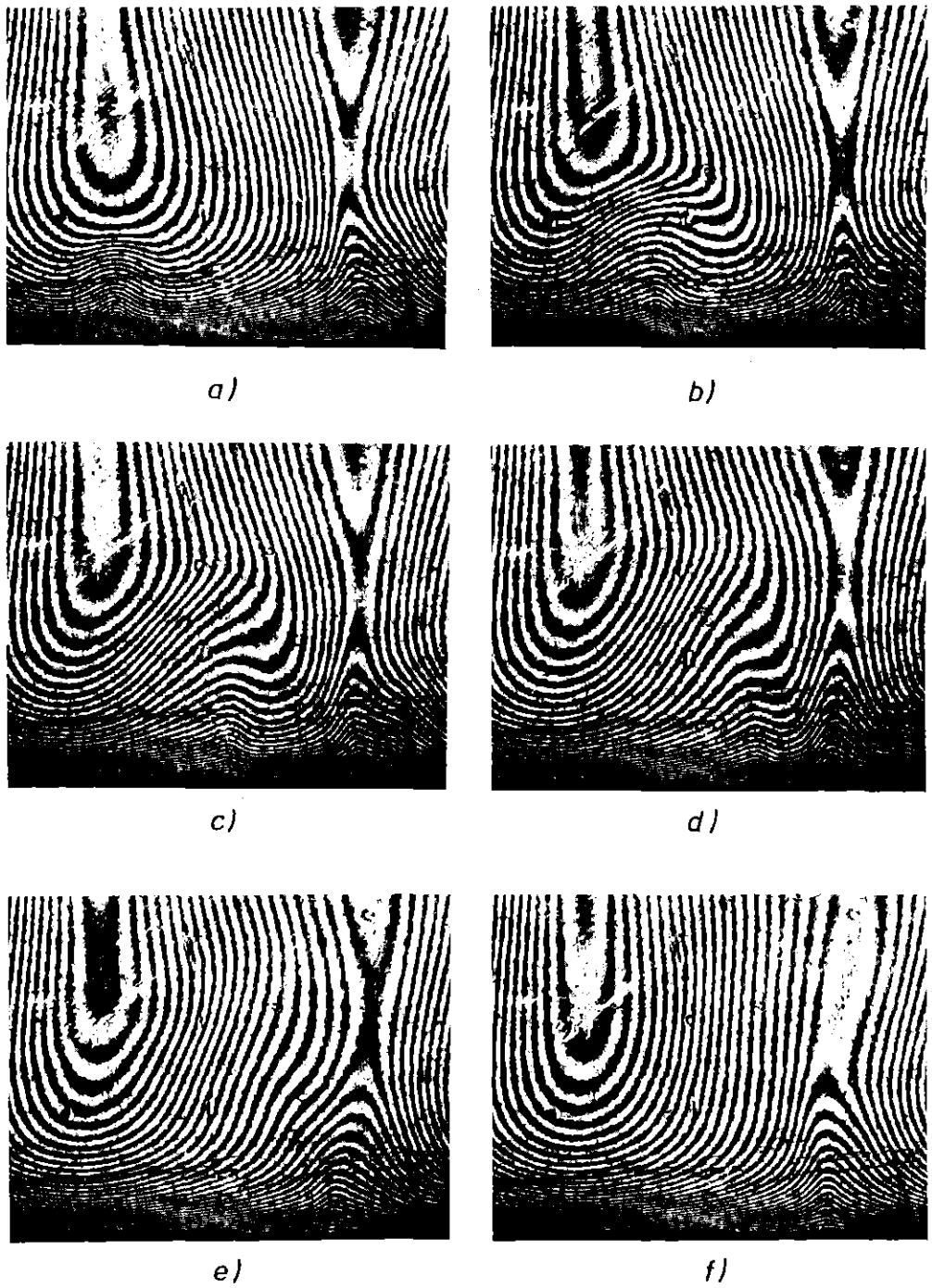

Figure 7: Interferogram sections demonstrating instability of the temperature boundary layer at the bottom of a Hele-Shaw cell at Ra/Ra_c = 11.8. Hele-Shaw cell with plexi glass walls, water as test fluid and aspect ratios h/d = 66.5, h/b = 0.15. Time intervall a) - f) 240 seconds.

zontal wall wave like perturbations occur close to the position of downward convection. These perturbation are circulated sidewise and finally upwards by the mean flow within each convection cell. The process is repeated periodically and can be explained as an instability of the temperature boundary layer at the heated and/or cooled lower and upper boundaries of the fluid layer. Such instability events occur in each cell. The coherence between the events in neighbouring cells is smal, if existent at all.

Careful regions observations of real time interferograms have revealed moreover, that the regions of up and down flow in the Hele-Shaw cell i. e. the interior boundaries of the convection cell fluctuated about a certain value. These fluctuations seemed to be not directly correlated to the periodic events of the temperature boundary layer of neighbouring cells. Nevertheless it is hypothesized, that a weak interaction of wave like disturbances from several neighbouring cells initiate the fluctuations.

For a detailed study of these phenomena two thermocouples were placed into the boundary layer at the lower horizontal wall. One thermocouple was positioned close to the downflow stagnation point the other near to the upflow stagnation point. Typical time histories and their Fourier spectra for different Rayleigh numbers (the Rayleighnumber Ra^* is a normalized value related to the onset of unsteady convection $Ra^* = Ra/Ra_{osc}$) can be seen in fig. 8. The periodic event at the onset of unsteady convection can be recognized from the temperature history as well as from the frequency peaks in the power spectra for $Ra^* = 1.05$. The noise level apparent already in the spectrum at the onset of oscillation rises and broadens around the frequency peaks at moderately higher Rayleigh numbers. Predomenant frequencies can nevertheless be determined from the maxima in the power spectra corresponding to thermocouples sensing the down flow in the cell[1)]. The spectra

1) For Rayleigh numbers close to the threshold of oscillatory flow the spectra acually reveal a biperiodic oscillation (see fig. 8, $Ra^* = 1.64$). It is hypothesised, that the biperiodic character is caused by a synchronisation of two instability events in the same or in neighbouring cells.

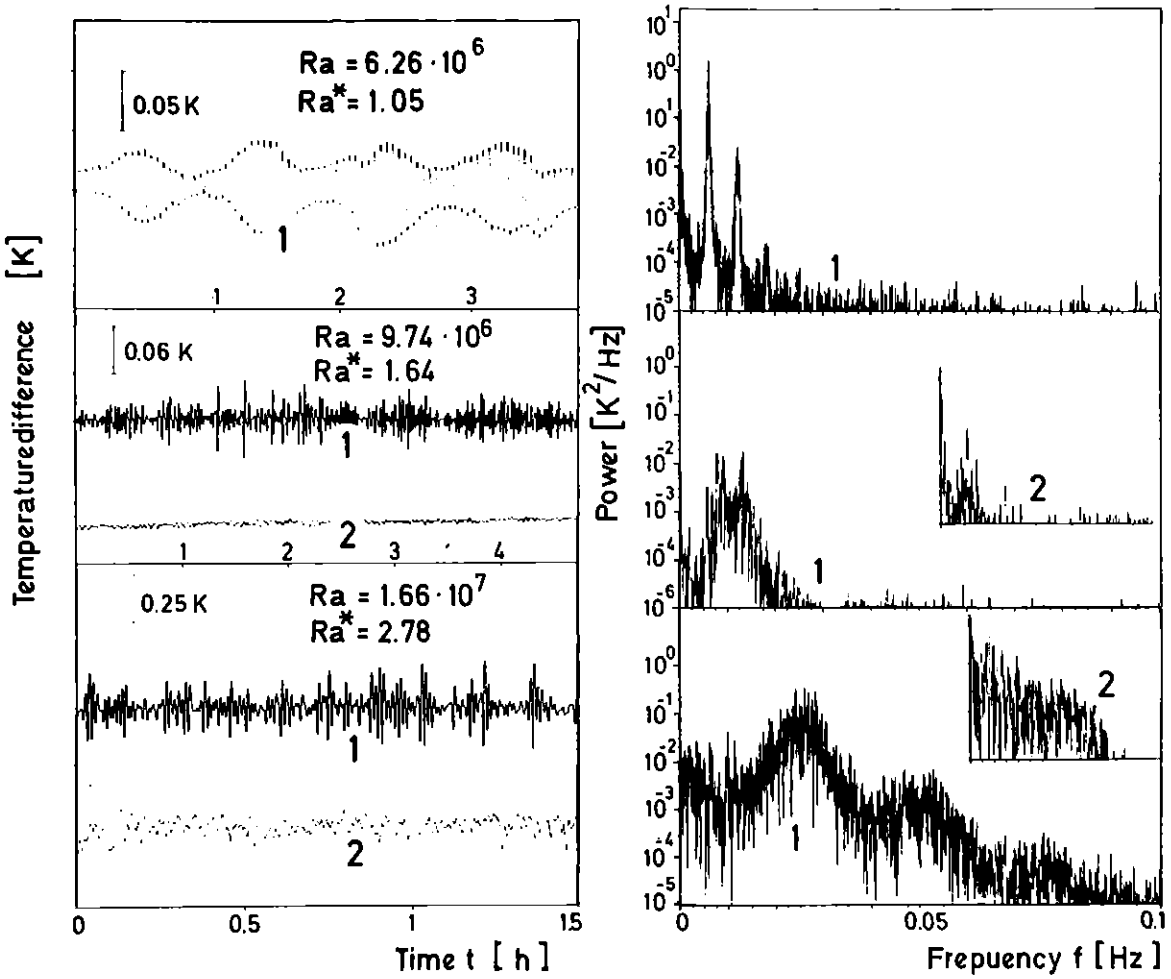

Figure 8: Temperature histories and power spectra of oscillatory convection in a Hele-Shaw cell (geometrical measures as given in fig. 6) for different Rayleigh numbers.

1 signals from thermocouple located near downstream stagnation point.

2 signals from thermocouple placed near upstream stagnation point.

corresponding to thermocouples sensing the upwards flow exhibit low frequency broad band noise. This indicates, that a strong influence from the instability events in the neighbouring cell does not exist.

The phenomena realized by visual observations and signal analysis suggest the following process for the transition from steady to unsteady convection in a Hele Shaw cell of large aspect ratio: The unsteady convection is initiated by an instability of the temperature boundary layer and features periodicity. Stochastic fluctuation of the size of convection cells are strongly excited by the boundary layer instabilities when the Rayleigh numbers are increased beyond the threshold for boundary layer instability. These fluctuations cause broad band noise in the spectra concealing the periodic events due to boundary layer instabilities. Similar explanations have been given by /62, 87/, which were concluded from numerical calculations based on the model equations for convection in porous media.

A high sensitivity of free convection to low frequency fluctuations and broad band noise in containers of large aspect ratio has been observed by other researchers /60, 61, 67/. Though a direct comparison cannot be drawn because of the difference in the geometries (Hele-Shaw cells, cylindrical cavity) it is suggested that the broad band spectra have the same origin namely cell size fluctuations /9/ triggered by a great many of weakly or even uncorrelated instability events in the temperature boundary layers of different convection cells.

From the power spectra single frequencies can nevertheless be attributed to peaks and maxima in the spectra. In fig. 9 dimensionless oscillation periods corresponding to the most energetic frequencies characterized by peaks and maxima in the spectra are given as a function of the related Rayleigh number Ra^*. The periods of oscillation decrease with increasing Rayleigh number. The power law describing the decrease in the oscillation time changes, from Ra^{-2} to Ra^{-1}. This behaviour can be well explained by simple similarity arguments /65/. Assuming that at the onset of unsteady

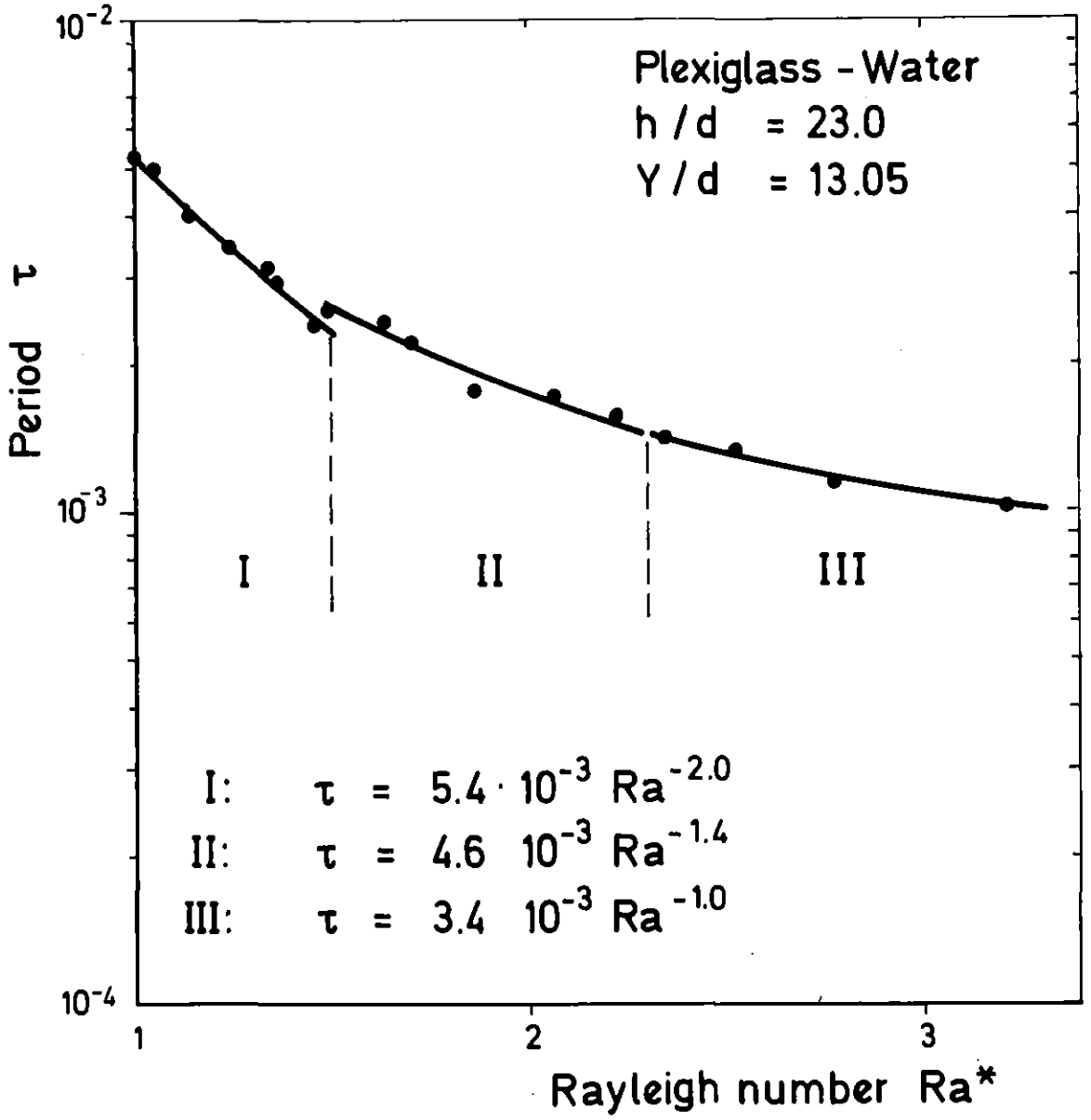

Figure 9: Dimensionless oscillation periods τ of most energetic frequencies in power spectra versus normalized Rayleigh number $Ra = Ra/Ra_{osc}$.
$\tau \sim t(h^2/\kappa)$, h - height of Hele-Shaw cell, κ - thermal diffusivity of test liquid, t - phyiscal time, Ra_{osc} - Rayleigh number at onset of oscillation, geometry of Hele-Shaw cell as given in fig. 6.

convection the thickness of the temperature boundary layer is still considerably larger than the depth of the Hele-Shaw cell and employing the stability criterium for Bénard convection in gaps the power low $\tau \sim Ra^{-2}$ is immediately confirmed. At higher Rayleigh numbers the thickness of the temperature boundary layer decreases and for the stability criterium a Rayleigh number as defined for infinite layers is becoming more appropriate. Similar arguments would then lead asymptotically to the well known correlation $\tau \sim Ra^{-2/3}$ which is due to instabilities in the temperature boundary layer in infinitely extended fluid layers /65/. The actual curve has to fall in between these two limiting cases.

Thus the power laws found from the experiments and explained by similarity arguments underline the stability mechanism at the threshold of unsteady convection in Hele-Shaw cells.

4.3 The Hele-Shaw Cell of Small Aspect Ratio (Hele-Shaw Slot)

4.31 Flow Pattern

The spacial structures of the Bénard convection in Hele-Shaw slots of five different aspect ratios (A = 14; 7; 4.7; 3.5; 1.75; A=gap height to gap width)[1)] was visualized employing holographic interferometry. The experiments were performed in Hele-Shaw slots with either well or with poorly conducting side walls (crystal glass and silicon oil plexiglass and water). In the range of Rayleigh numbers $10^7 \leq Ra \leq 4 \cdot 10^8$ five qualitatively different flow pattern have been observed. For aspect ratios 3.5 and 4.7 typical interferograms as well as schematic illustrations of corresponding streamlines are given in fig. 10. Single (a), double (c), and vertically ordered (b) steady state convection rolls can be found at transcritical Rayleigh numbers depending on the heating history. The steady state convection is replaced by an oscillatory flow at a threshold Rayleigh number which depends on the aspect ratio. Like in the case of Bénard convection in Hele-Shaw cells the unsteady flow is induced by unstable temperature boundary layers at top and bottom of the slot, from which blobs of hot or cold fluid are released. These hot and cold blobs first rise and fall along the

1) Height to depth ratio h/d = 23.3

side walls and then generate a highly unsteady mixing zone in the middle part of the Hele-Shaw slot. An instantaneous interferogram of this oscillatory state is shown in fig. 10d. More details of the periodic character of this type of flow can be seen in fig. 11a and 11b, where one period of the flow oscillation is described by a series of interferograms. From the interferograms in fig. 11a the high degree of spacial symmetry can be recognized which is typical for Rayleigh numbers just beyond the threshold of unsteady flow. As can be seen from figure 11b this symmetry is lost at higher Rayleigh numbers.

At very high supercritical Rayleigh numbers a relaminarization[1)] of the flow oscillatory occurs. This state can be best described as a four roll steady state convection as indicated by the stream line pattern in fig. 10e.

Relaminarisation of oscillatory convection (state c in fig. 10) as well as the occurrance of vertically ordered double roll system (state b in fig. 10) are phenomena, which are due to the lateral confinement of the fluid layer and are strongly correlated to the aspect ratio. Decreasing the height to width ratio of the Hele-Shaw slot (i. e. increasing the degree of freedom for the convective flow) reduces the probability of the occurrance of such states. Thus a vertically ordered double roll system could only be observed during the experiments in Hele-Shaw slots of aspect ratio A = 4.7 and the four roll system steady state could not be realized in Hele-Shaw cells with A = 1.7.

---

1) The concept of relaminarization is used here in the sense, that no signals below the response time of the thermocouples (6 Hz), which were used for signal detection in the experiments, were registered.

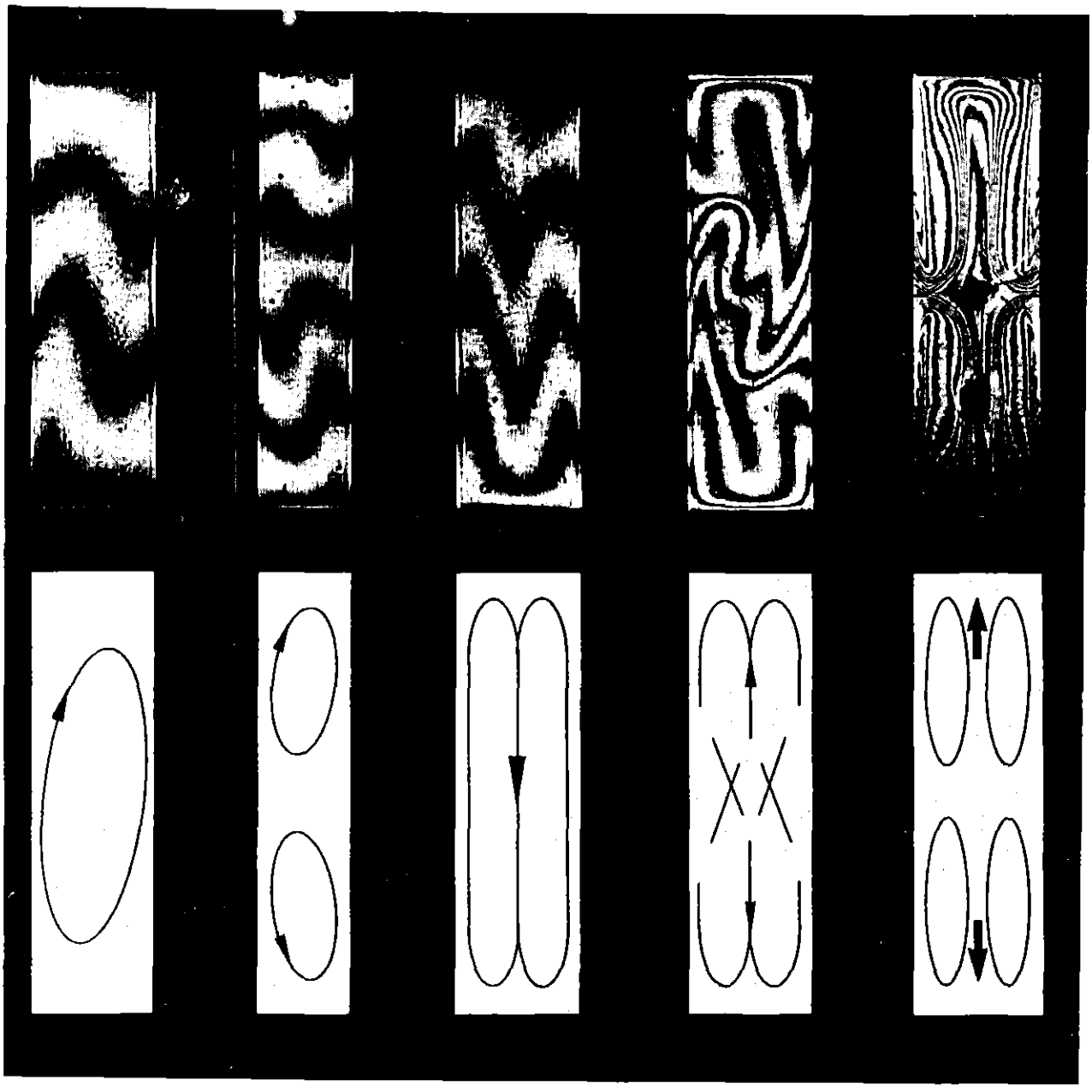

Figure 10: Different flow patterns in Hele-Shaw slots with high conductivity side walls (combination glass walls - solocone oil) for Rayleigh numbers; a) $Ra_{c1} = 1.3 \cdot 10^7$, b) $Ra = 3.4 \cdot 10^7$ (Ra_{c2} not exactly determined), c) $Ra_{c2} = 2.4 \cdot 10^7$, d) $Ra_{c3} = 4.9 \cdot 10^7$, e) $Ra_{c4} = 3.5 \cdot 10^7$.

4.32 Temporal Structure of Oscillatory Convection in Hele-Shaw Slots

As the unsteady oscillatory convection prevailed for moderate aspect ratios and for a large range of supercritical Rayleigh numbers, this type of flow has been explored in detail by visual observation and by signal analysis from local temperature probes /56/. The investigations were mainly aimed at finding out influences of aspect ratios, thermal properties of the side walls as well as Rayleigh numbers upon the spacial and temporal structure of the unsteady flow. Therefore the experiments were carried out in Hele-Shaw slots of different aspect ratios and with confining side walls of well conducting (crystal glass - silicon oil) and poorly conducting (plexi glass - water) materials.

First a more detailed discussion of the flow oscillations in a Hele-Shaw slot of aspect ratio 3.5 and good conductivity side walls shall be given. In fig. 12 the dimensionless oscillation period is plotted as a function of the normalized Rayleigh number $Ra^* = Ra/Ra_{osc}$.

The results of this graph were obtained from Fourier spectra of temperature signals. The temperature was measured by thermocouples placed into the mixing zone in the middle part of the container. Only the most energetic frequencies of the spectra and subharmonics of them are listed.

The graph shows the following gross features:

- The periods of flow oscillations decrease with increasing Rayleigh numbers. This decrease levels off to a plateau at higher Rayleigh numbers. A frequency cut off occurs at nine times the Rayleigh number of onset of oscillatory convection. This phenomena indicates the transition from an unsteady periodic flow to a steady state four roll convection pattern (see fig. 10e).

- At the beginning as well as at the end the range of oscillatory flow exhibits a hysteresis. (The hysteresis effect at the onset of oscillations is not marked in this graph but see /56/ for details.)

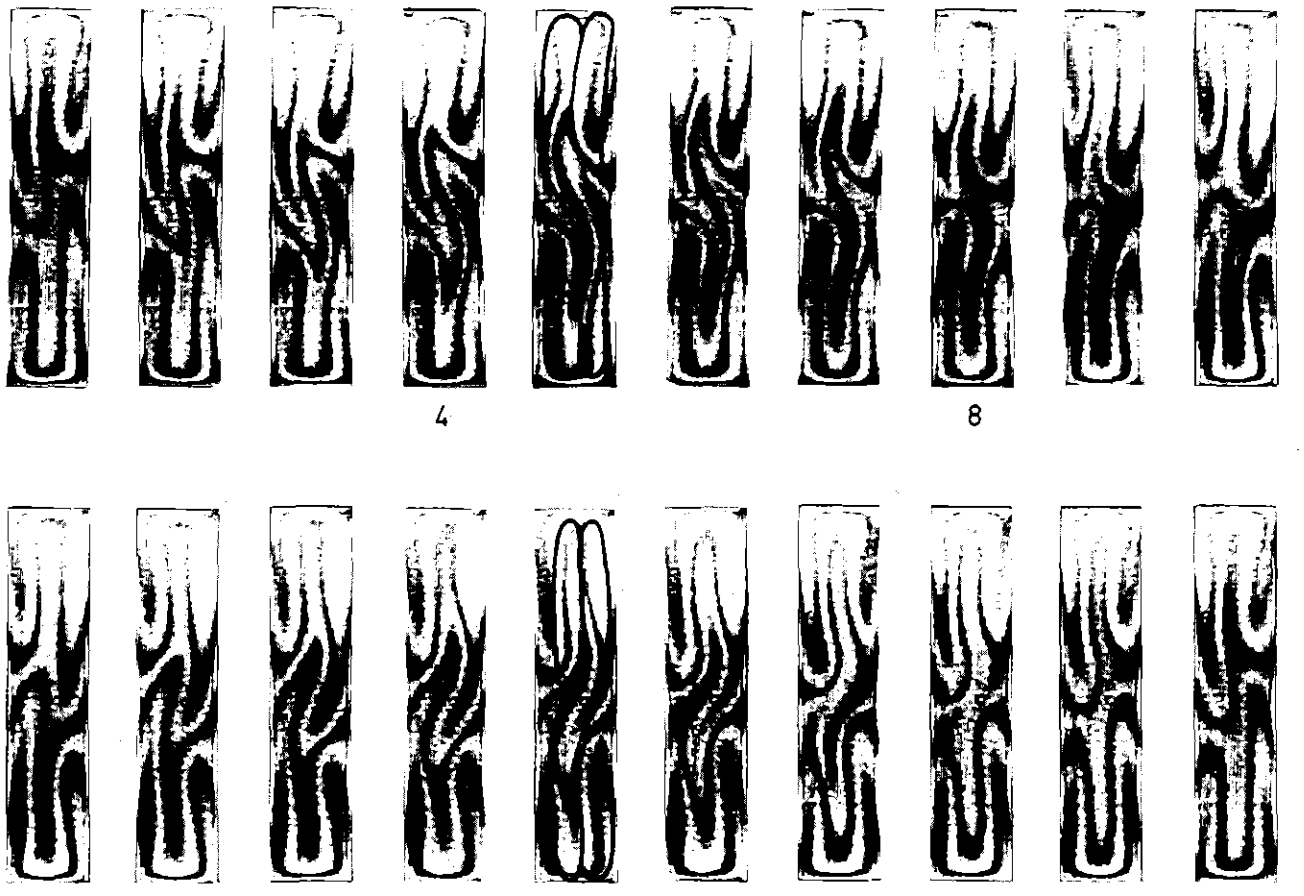

Figure 11a: Interferograms in chronological order representing one oscillation period:
a) periodic oscillations and spacially symmetric flow pattern, aspect ratio $h/b = 4.7$, $Ra^* = 1.01$, ($Ra_{osc} = 5.7 \cdot 10^7$).

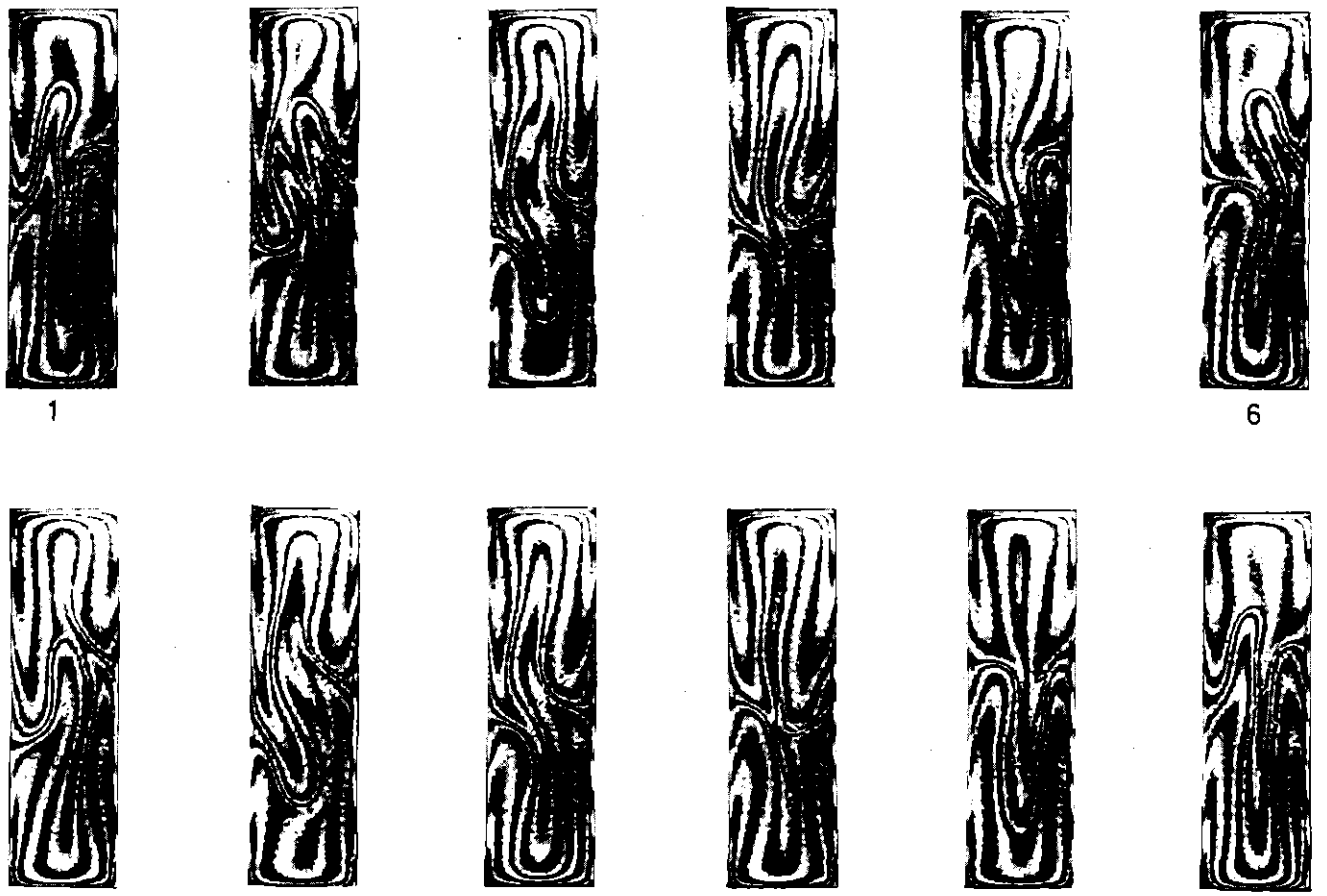

Figure 11b: Interferograms in chronological order representing one oscillation period:

b) biperiodic oscillation (synchronized) and aspacially nonsymmetric flow pattern, aspect ratio h/b = 3.5, Ra* = 1.6.

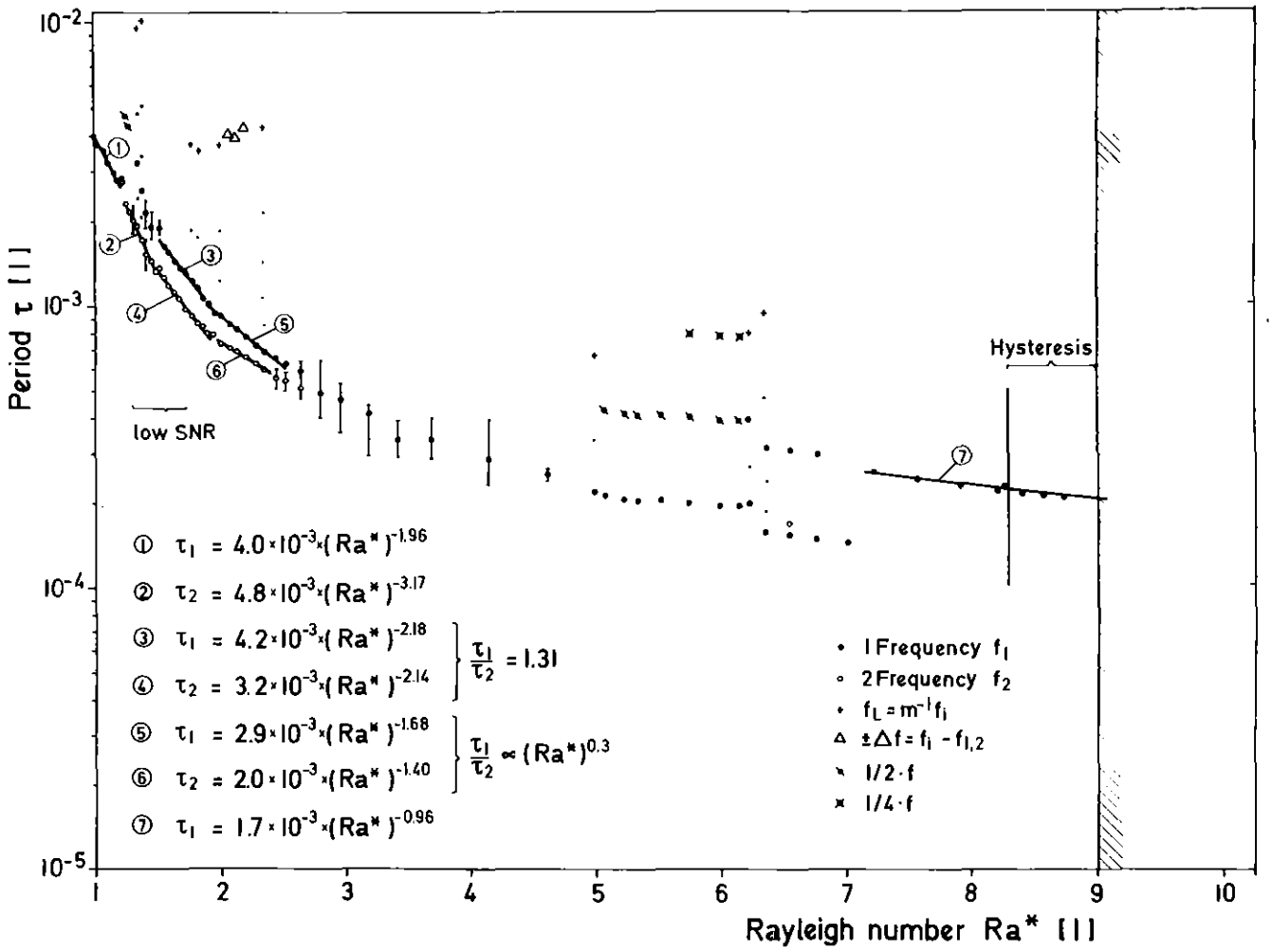

Figure 12: Dimensionless oscillation period versus normalized Rayleigh number Ra^* in Hele-Shaw slot h/b = 3.5, h/d = 22.6 with high conductivity side walls; Pr = 36.5.

- From the corresponding power spectra it can be realized, that in the range of Rayleigh numbers, where oscillatory flow occurs, repeatedly states of higher order (characterized by line spectra) are replaced by states of lower order (characterized by line spectra with a high noise level or even by broad band spectra) and vice versa. Typical samples of temperature histories and spectra are shown in fig. 13. Totally seven intervals of order and six 'noisy' intervals have been found in the present case.

Besides these gross features the diagram contains the following details related to the fine structure of the oscillatory flow:

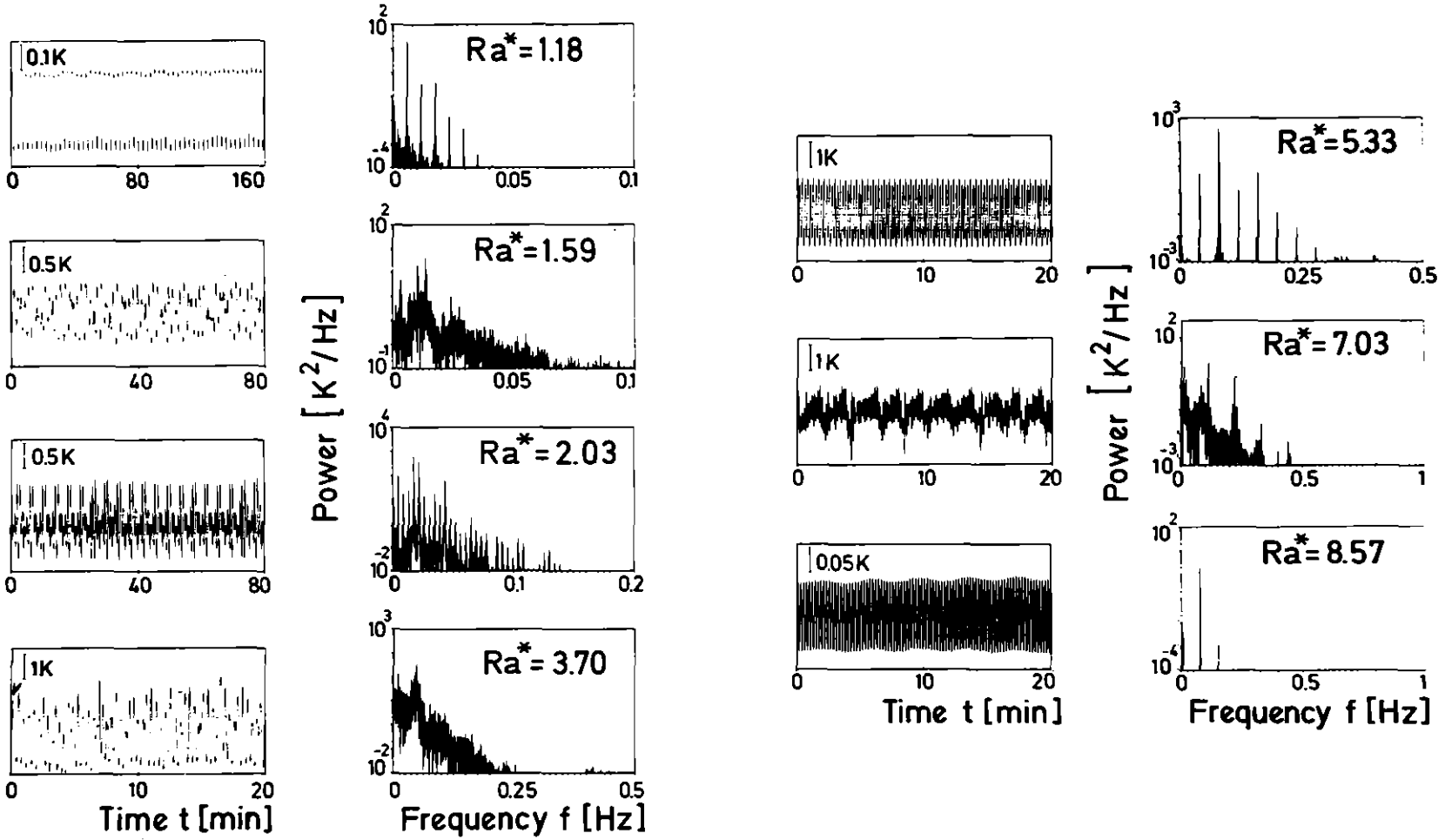

Figure 13: Typical power spectra and temperature histories for Hele-Shaw slots with high conductivity side walls and aspect ratios h/b = 3.5, h/d = 22.6 (Pr = 36.5).

- At onset the unsteady flow is time periodic ($1 < Ra^* < 1.18$). The power law $\tau \sim Ra^{-2}$ indicates, that the oscillations originate from an instability of the temperature boundary layer.
- Subharmonic frequency partition ($Ra^* = 1.25$) preceeds the occurrance of biperiodic (quasiperiodic) oscillations ($1.55 < Ra^* < 2.54$). In the biperiodic range repeatedly frequency locking (synchronization) occurs. The locking processes results in general in well ordered oscillations (line spectra), which differ from neighbouring states by a considerable lower noise level in the spectra.
- Stochastic oscillations succeed the biperiodic ones in the range $2.6 < Ra^* < 4.6$. These stochastic oscillations are characterized by broad band spectra.
- The range of stochastic oscillations is terminated by a reemerging periodic oscillation containing several subharmonics in the spectra ($Ra^* = 5.1$).
- The periodic oscillation approaches closely a harmonic oscillation before the cut off occurs at $Ra^* = 9$.

From the study of convection in Hele-Shaw slots of different side wall materials it has been found moreover that the general spacial and temporal character of the flow oscillations is very similar in slots with high and slots with low conductivity side walls.

The following specific features shall be mentioned, however:
- Low conductivity side walls reduce the threshold of onset of steady and of oscillatory convection and delay the transition from unsteady to a relaminarized four roll steady state convection. They favour, moreover, the formation of spacial nonsymmetric flow pattern and the occurance of oscillations with stochastic features.
- High conductivity side walls exert a damping effect on the oscillations and reduce stochastic fluctuations in the flow.
- Increasing the aspect ratios reduces generally the spacial and temporal order (periodicity, symmetry) of the convective flow for all Rayleigh numbers beyond the threshold of onset of oscillations. The threshold Rayleigh number for onset of oscillation is reduced if the aspect ratio is enhanced (see fig. 14).

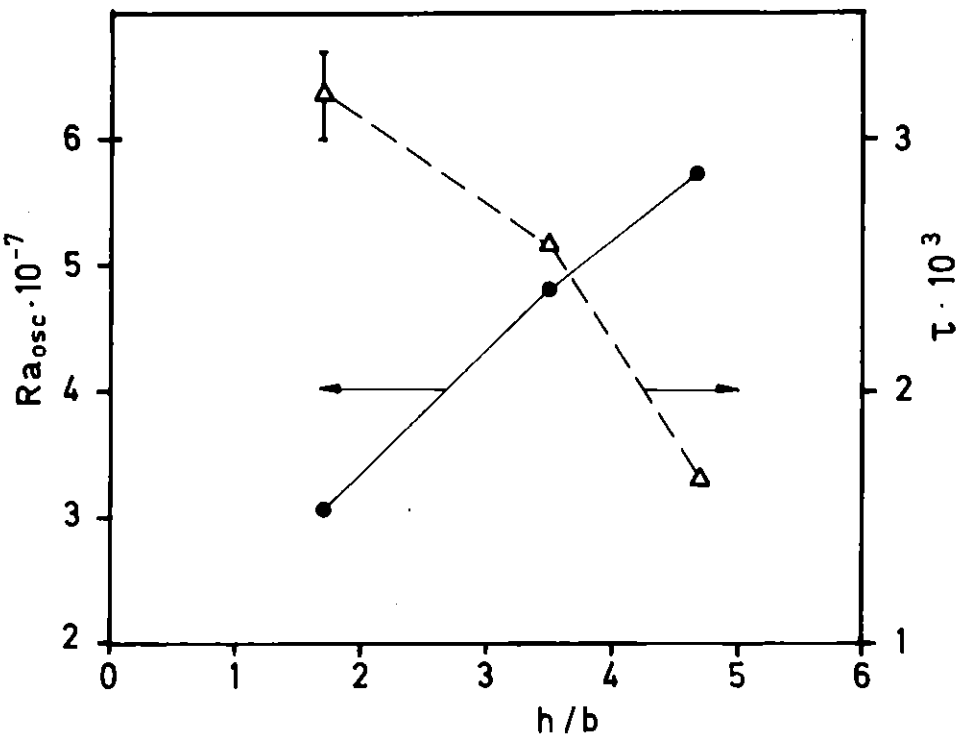

Figure 14: Threshold Rayleigh numbers Ra_{osc} and dimensionless Oscillation period τ for onset of oscillatory flow versus the aspect ratio h/b of the Hele-Shaw slot.

The general features of the oscillatory convection in the Hele-Shaw slot as outlined here are very similar to what has been observed and analysed by other researchers from Bénard convection in rectangular and cylindrical cavities of small aspect ratio /59,67/ (see chapter 3.3). For certain phenomena such as threshold for biperiodic flow oscillations and related first appearance of subharmonic frequency partition even quantitative agreement exists with findings of other researchers /55, 59, 67, 71/.

Though the temperature signals and their spectra seem to have a complex behaviour, the interferograms reveal comparatively highly structured patterns. From interferogram analysis the following mechanistic explanation is suggested for the physical processes.

In the Hele-Shaw slot of small aspect ratio the experimentally realized steady state convection preceding the oscillatory flow consists in general of two horizontally ordered rolls (fig. 10c). The temperature boundary layers on top and bottom of the slot can become unstable in each of these rolls. Because of the small aspect ratio at first the occurrance of wave like disturbances in

the temperature boundary layers succeeded by rising and falling blobs alternates between the two rolls with a phase shift of π. The alternating process induces a periodic oscillation with complete spacial symmetry (see fig.11a). If the Rayleigh number is increased beyond the threshold of onset of osczillation the phase shift in the blob release between the two convection rolls is reduced. Finally the two blobs within the different rolls are released from the lower or upper temperature boundary layer almost simultaneously. These events then alternate between the lower and the upper boundary of the slot. Phase shift reduction is directly linked to the occurrance of a second frequency in the temperature history and the corresponding power spectrum. Combined with the reduced phase shift a spacial asymmetry in the flow pattern becomes apparent (see fig. 11b). The experimental findings indicate, that for side walls of high conductivity the phase shift for blob release first occurs at another higher threshold Rayleigh number, whereas for low condutivity sid walls the reduction in phase shift is a smooth process /56/. Moreover in general the phase shift between the two instability events may vary within certain bounds for one definite Rayleigh number, however, synchronisation can occur for certain combinations of aspect ratios and Rayleigh numbers (and certain spacial symmetries depending on the interacting spacial modes).

Finally at very high Rayleigh numbers the oscillations die off, because the boundary layer instabilities disappear. The latter effect occurs because the thickness of the temperature boundary layers become comparable with the gap depth and a considerable amount of heat is withdrawn from the boundary layers by the side walls via conduction. Thus disturbances of the small scale are damped out by dissipation. In conclusion it is suggested, that recursive instabilities of temperature boundary layers induce flow oscillations in a bounded liquid continuum with nonlinear properties. Thus properties like subharmonic frequency partition known from forced nonlinear vibrations in mechanics /84/ are general properties not linked to a spacial geometry or Rayleigh number (amount of external stress to the system, see also /82, 83/).

4.4 Theoretical Models

The description of unsteady convection in gaps can be reduced essentially to two dimensions. Thereby experimental investigations can be supported by numerical calculations based on the Boussinesq equation and corresponding boundary conditions at the side walls.

As gap flow is two-dimensional, numerical calculations can be performed up to high Rayleigh numbers and for different parameters without serious limitations by available computing time. Such calculations have been performed using a Galerkin procedure as well as using a finite difference method /62, 68, 69, 72, 87/.

These calculations have confirmed characteristic phenomena of oscillatory flow in Hele-Shaw cells and Hele-Shaw slots.

Numerical calculations using either of the two numerical methods have shown, that the onset of flow oscillations is caused by wave like disturbances in the temperature boundary layers on the heated or cooled horizontal boundaries. These disturbances emerge periodically from the boundary layer periodically beyond a threshold Rayleigh number. Moreover, the calculations suggest that the events are harmonic first but obtain a relaxation character at higher Rayleigh numbers /68/. The numerically obtained fields of isotherms agree well with those on the interferograms obtained from experiments.

Moreover it has been revealed from fields of calculated isotherms that in a single convection cell even two, locally displaced wave like disturbance of different strength can occur in the temperature boundary layer on top or bottom. This double event is then noticed as a second (in the case calculated, however, coupled) frequency in the Nusselt number history /68, 87/. These findings indicate that one of the possible causes for biperiodic oscillations in Hele-Shaw cells can be double instability events in the boundary layers of one single convection cell[1)].

1) The biperiodic character of unsteady flow in Hele-Shaw cells has also been detected from the spectra of the temperature histories for a certain range of supercritical Rayleigh numbers beyond the threshold of onset of unsteady flow. However, due to a low signal to noise ratio in the spectra final conclusions related to this phenomena have not been drawn.

The calculations for Hele-Shaw slots employing in fig. 15b finite difference methos have reproduced essential phenomena observed in the experiments /72/. For instance the typical symmetric four roll oscillation is obtained. This is demonstrated in fig. 15b. Furthermore it was found that at a certain higher Rayleigh first the symmetry in time is lost as the oscillation becomes oriented to one side (see fig. 15b). This loss of symmetry is linked to a normal bifurcation of the periodic solution. At even higher Rayleigh numbers also the spacial symmetry at each instant of time gets lost. The calculations shows, that this loss of symmetry goes again together with a bifurcation of the oscillatory solution. Like in the experimental findings, the transition from spacially symmetric to asymmetric patterns is linked to the occurance of a secondary frequencies in the local temperature and Nusselt number history.

Another spacially asymmetric oscillatory solution was found for the Rayleigh numbers below the threshold Rayleigh number for onset of symmetric oscillations. Detailed numerical studies have shown, that this solution branches off from the symmetric four roll oscillation (fig. 15b) in an inverted bifurcation.

The corresponding streamline and isotherm pattern is given in fig. 15a. As the threshold for branching is lower than the Rayleigh number for onset of oscillatory convection when the Rayleigh number is increased the hysteresis for the onset of oscillatory flow becomes apparent.

Similar hysteresis effects have also been found in the convection experiments in Hele-Shaw slots /56/.

In conclusion numerical calculations are able to describe a number of typical phenomena observed in free convection in Hele Shaw cells as well as Hele Shaw slots. Moreover, the calculation validize the assumption that the experimental phenomena have essentially a two-dimensional character.

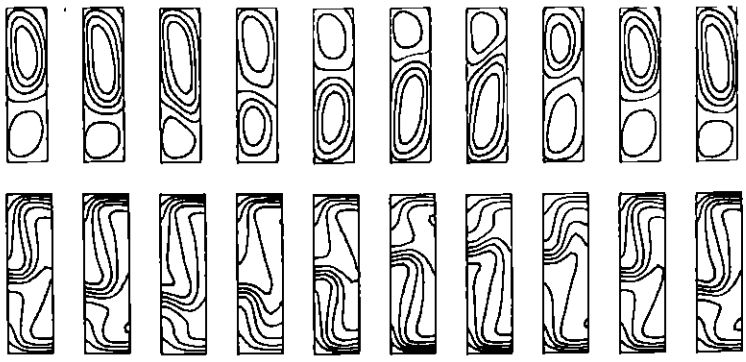

$Ra = 0.45 \cdot 10^7$

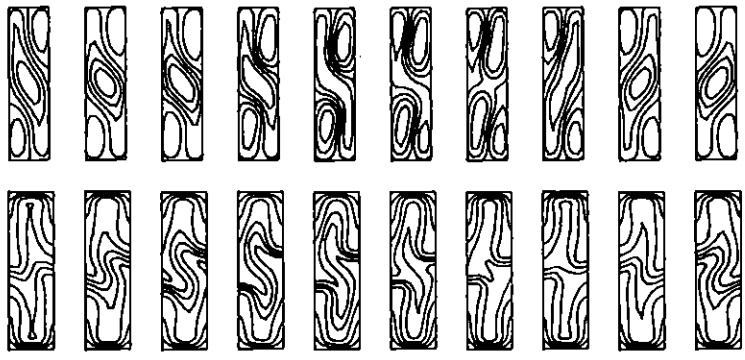

$Ra = 0.85 \cdot 10^7$

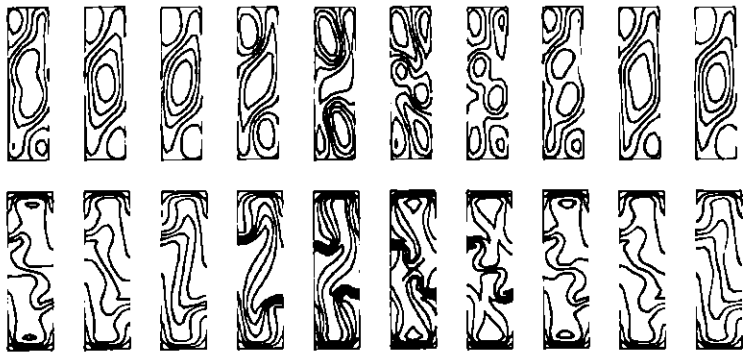

$Ra = 1.3 \cdot 10^7$

Figure 15: Typical streamline and isotherm patterns calculated in different ranges of Rayleigh numbers (adiabatic side walls)
a) for a range of spacially asymmetric flow below the threshold Rayleigh number for onset of oscillatory flow (range of hysteresis) $Ra = 0.45 \cdot 10^7$.
b) for the range of spacially symmetric oscillatory flow, $Ra = 0.85 \cdot 10^7$.
c) for a range of symmetric oscillatory flow, $Ra = 1.3 \cdot 10^7$.

5. Summary and Conclusions

As two-dimensional convective flow in gaps is a very simple hydrodynamic system, it proves to be very useful to study complex phenomena of unsteady cellular convection /62, 63, 64, 69, 77/. Combining visual observation of flow pattern by holographic interferometry, signal analysis from Fourier spectra of temperature histories and results from numerical calculations several phenomena of the complex unsteady flow can be correlated and to some extend mechanisticcally explained.

The initiating event for unsteady convection in gaps is an instability of the temperature boundary at the horizontal heated or cooled walls, which results generally at the beginning in a periodic flow oscillation.

The oscillations generally become biperiodic with increasing Rayleigh numbers. There are indications, that the second frequency in the oscillation can be caused by a second instability in the same roll cell (Hele Shaw cell event obtained from calculations /68/) or by quasy simultaneous release of blobs of hot or cold fluid from the unstable boundary layers in two neighbouring roll cells. (Hele Shaw slot event observed in experiments and simulated by calculation /56, 72.) This latter event is correlated to spacially asymmetric flow pattern.

The release processes in neighbouring cells may be bounded in a certain range of phase shift or may be synchronized depending on the Rayleigh number and the aspect ratio of the slot (quasi periodic behaviour or frequency locking).

For the Hele-Shaw cell the arising broad band noise following immediately the boundary layer instability events can be correlated to fluctuations of the free boundaries of the convection cells exited by the boundary layer instabilities. The systems sensitivity to fluctuations inturn is supposed to be caused by metastable state which is due to a wave number, aspect ratio and Rayleigh number mismatch in a finite system (more degrees of freedom compared to the slot geometry).

The stochastic oscillations of a flow in Hele Shaw slots are basically of the same origin. Their occurance at a higher Rayleigh number threshold as well as the possibility of reemergent ordered synchronized periodic oscillations underline the importance of matching between the parameters cell size of flow aspect ratio and Rayleigh number /62, 77/.

The results obtained so far are insufficient for immediate design work concerning the control of heat and mass transport in slender cavities. More work is required to quantify the correlation between flow pattern, aspect ratio, Rayleigh number, and thermal properties of the materials. Nevertheless, there are hints that flow oscillations can be controlled by choosing the parameters named properly.

Acknowledgements

The author appreciates valuable discussions with J. N. Koster, Cl. Günther, H. Frick and Ch. Dietsche during the preparation of this article.

He is indepted to Cl. Günther and D. W. Sallet for careful reading a draft of the manuscript and for valuable suggestions for improvements.

Figures: Legends

Fig. 1: Sketch of rectangular cavity.

Fig. 2: Critical Rayleigh numbers and flow pattern in a rectangular box. Aspect ratios for the critical Rayleigh numbers ($h_1 = \Gamma_x$, $h_2 = \Gamma_y$) $\Gamma_x = 6$, $0.6 < \Gamma_y < 6$, aspect ratio for flow pattern $\Gamma_x = 6$, $\Gamma_y = 3$.

Fig. 3: Influence length of lateral walls represented by velocity measurements within convection cells after /38/.

Fig. 4: Smooth transition from rest to finite amplitude convection (solid line) in contrast to sharp transition (dashed line) after /46/.

Fig. 5: Critical Rayleigh numbers for Hele-Shaw cells of different height to depth ratios h/d and different side wall materials. For comparison see theoretical results of /18/ and /80/.

Fig. 6: Stability map of two-dimensional convective flow in a Hele-Shaw cell in reduced variables Ra/Ra_c, α/α_c, Ra_c - critical Rayleigh number and α_c - critical wave number at onset of convection. Experiments were performed in a Hele-Shaw cell with plexi glass walls, water as a test fluid and aspect ratios h/d = 41, h/b = 0.095. Lines correspond to theoretical results /68, 69/ dots experimental results /56/.

Fig. 7: Interferogram sections demonstrating instability of the temperature boundary layer at the bottom of a Hele-Shaw cell at $Ra/Ra_c = 11.8$. Hele-Shaw cell with plexi glass walls, water as test fluid and aspect ratios h/d = 66.5, h/b = 0.15. Time intervall a)-f) 240 s.

Fig. 8: Temperature histories and power spectra of oscillatory convection in a Hele-Shaw cell (geometrical measures as given in fig. 6) for different Rayleigh numbers.
1 signals from thermocouple located near downstream stagnation point,
2 signals from thermocouple placed near upstream stagnation point.

Fig. 9: Dimensionless oscillation periods τ of most energetic frequencies in powes spectra versus normalized Rayleigh number $Ra = Ra/Ra_{osc}$.
$\tau = t(h^2/\kappa)$, h - height of Hele Shaw cell, κ - thermal diffusivity of test liquid, t - physical time, Ra_{osc} - Rayleigh number at onset of oscillation, geometry of Hele-Shaw cell as given in fig. 6

Fig. 10: Different flow patterns in Hele Shaw slots with high conductivity side walls (combination glass walls - silicon oil) for Rayleigh numbers; a) $Ra_{c1} = 1.3\ 10^7$, b) $Ra = 3.4\ 10^7$ Ra_{c2} not exactly determined), c) $Ra_{c2} = 2.4\ 10^7$, d) $Ra_{c3} = 4.9\ 10^7$, e) $Ra_{c4} = 35.7\ 10^7$.

Fig. 11: Interferogramms in chronological order representing one oscillation period:
a) periodic oscillations and spacially symmetric flow pattern, aspect ratio h/b = 4.7, $Ra^* = 1.01$, ($Ra_{osc} = 5.7\ 10^7$).
b) biperiodic oscillation (synchronized) and spacially nonsymmetric flow pattern, aspect ratio h/b = 3.5, $Ra^* = 1.6$.

Fig. 12: Threshold Rayleigh numbers Ra_{osc} and dimensionless oscillation period τ for onset of oscillatory flow versus the aspect ratio h/b of the Hele Shaw slot.

Fig. 13: Dimensionless oscillation period versus normalized Rayleigh number Ra^* in Hele-Shaw slot h/b = 3.5, h/d = 22.6 with high conductivity side walls, Pr = 36.5.

Fig. 14: Typical power spectra and temperature histories for Hele-Shaw slots with high conductivity side walls and aspect ratios h/b = 3.5, h/d = 22.6 (Pr = 36.5).

Fig. 15: Typical streamline and isotherm patterns calculated in different ranges of Rayleigh numbers (adiabatic side walls)

a) for the range of spacially symmetric oscillatory flow, $Ra = 0.6\ 10^7$.

b) for a range of a symmetric oscillatory flow, $Ra = 1.3\ 10^7$.

c) for a range of spacially asymmetric flow below the threshold Rayleigh number for onset of oscillatory flow (range of hysteresis) $Ra = 0.42\ 10^7$.

References

/1/ D. Japikse:
Advances in Thermosyphon Technology;
Advances in Heat Transfer 1973, Ed. Th.F. Irvene, J.P. Hartnett, Academic Press.

/2/ D.K. Edwards, J.N. Arnold, I. Catton:
End-Clearance Effects on Rectangular Honeycomb Solar Collectors;
Solar Energy 18, 253-257, 1976.

/3/ F. Rosenberger:
Fundamentals of Crystal Growth;
Springer 1959.

/4/ D. Ruelle, F. Takens:
On the Nature of Turbulence;
Commun Math. Phys. 20, 168-192, 1972.

/5/ P.C. Martin:
Instabilities, Oscillations, and Chaos;
Journ. de Phys. Coll. C1., Janv. 1976, C1-57.

/6/ M.J. Rabinovich:
Stochastic Self-Oscillations and Turbulence;
Sov. Phys. Usp. 21(5), 123-168, May 1978.

/7/ J. P. Gollub:
The Onset of Turbulence: Convection, Surface Wave, and Oscillators;
Systems Far from Equilibrium, Ed. L. Garrido, Lecture Notes in Physics 132, Springer 1980.

/8/ G. Ahlers:
Onset of Convection and Turbulence in a Cylindrical Container
Systems Far from Equilibrium, Ed. L. Garrido, Lecture Notes in Physics 132, Springer 1980.

/ 9/ P. Bergé:
Experiments on Hydrodynamic Instabilities and Transition to Turbulence;
Dynamical Critical Phenomena and Related Topics, Proc. Geneva 1979, Ed. C.P. Enz. (to be published).

/10/ J.M. Olson, F. Rosenberger:
Convective Instabilities in a Closed Vertical Cylinder Heated from Below, Part 1: Monocomponent Gases;
J. Fluid Mech. 92, 609-629, 1979.

/11/ R.K. Sobermann:
Effects of Lateral Boundaries on Natural Convection;
J. of Appl. Physics 29, 872-873, 1958.

/12/ E.L. Koschmieder:
On Convection on a Uniformly Heated Plane;
Beiträge zur Physik der Atmosphäre 39, 1-11, 1966.

/13/ D.D. Joseph:
Stability of Convection in Containers of Arbitrary Shape;
J. Fluid Mech. 47, 257-282, 1971.

/14/ S. Chandrasekhar:
Hydrodynamic and Hydromagnetic Stability;
Oxford 1961.

/15/ G.Z. Gershuni, E.M. Zhukhovitskii:
Convective Stability of Incompressible Fluids;
Ketr Press Jerusalem, 1976.

/16/ J. Zierep:
Zur Theorie der Zellularkonvektion V;
Betr. Phys. Atmos. 36, 70-76, 1963.

/17/ S. Ostrach, D. Pnueli:
J. Heat Transfer, 346-354, Nov. 1963.

/18/ H. Frick, R.M. Clever:
Einfluß der Seitenwände auf das Einsetzen der Konvektion in einer horizontalen Flüssigkeitsschicht;
ZAMP 31, 502-513, 1980.

/19/ S.H. Davis:
Convection in a Box: Linear Theory;
J. Fluid Mech. 30, 465-478, 1967.

/20/ K. Stork, U. Müller:
Convection in a Box: Experiments;
J. Fluid Mech. 54, 599-611, 1972.

/21/ L.A. Segel:
Distant Side-Wall Cause Slow Amplitude Modulation of Cellular Convection;
J. Fluid Mech. 38, 203-224, 1969.

/22/ R.P. Davis-Jones:
Thermal Convection in an Infinite Channel with no Slip Side Walls;
J. Fluid Mech. 44, 695-704, 1970.

/23/ G.S. Charlson, R.L. Sani:
Thermoconvective Instability in a Bounded Cylindrical Fluid Layer;
Int. J. Heat Mass Transfer 13, 1479-1496, 1970.

/24/ G.S. Charlson, R.L. Sani:
On Thermoconvective Instability in a Bounded Cylindrical Fluid Layer;
Int. J. Heat Mass Transfer 14, 2157-2160, 1971.

/25/ K. Stork, U. Müller:
Convection in Boxes: An Experimental Investigation in Vertical Cylinders and Annuli;
J. Fluid Mech. 71, 231-240, 1975.

/26/ E.L. Koschmieder, S.G. Pallas:
Heat Transfer Through a Shallow Horizontal Convecting Fluid Layer;
Int. J. Heat Mass Transfer 17, 991-1002, 1974.

/27/ K.R. Kirchartz, U. Müller, H. Oertel, J. Zierep:
Axisymmetric and Non-Axisymmetric Convection in a Cylindrical Container;
to appear in Acta Mechanica, 1981.

/28/ W.T. Mitchel, J.A. Quin:
Thermal Convection in a Completely Confined Fluid Layer;
A.I.Ch.E. Journal, 1116-1123, Nov. 1966.

/29/ C.A. Jones, D.R. Moore:
The Stability of Axisymmetric Convection;
Geophys. Astrophys. Fluiddyn., 2, 245-270, 1979.

/30/ G.R. Charlson, R.L. Sani:
Finite Amplitude Axisymmetric Thermoconvective Flows in a Bounded Cylindrical Layer of Fluid;
J. Fluid Mech. 71, 209-229, 1975.

/31/ K. Stork:
Zellularkonvektion in Behältern und in geschichteten Flüssigkeiten;
Dissertation Universität Karlsruhe, 1974.

/32/ F.B. Lipps:
Numerical Simulation of Three-Dimensional Bênard Convection in Air;
J. Fluid Mech. 75, 113-148, 1976.

/33/ H. Oertel:
Three-Dimensional Convection Within Rectangular Boxes;
in: Natural Convection in Enclosures, Am. Soc. Mech. Eng. HTD-8, 11-16, 1980; 19th Nat. Heat Transf. Conf. Orlando, Florida, July 27-30, 1980.

/34/ I. Catton:
Natural Convection in Enclosures;
Proc. of the 6th Int. Heat Transf. Conf., Toronto, 6,13-30, 1978.

/35/ D.K. Edwards:
Suppression of Cellular Convection by Lateral Walls;
J. Heat Transfer, 145-150, Febr. 1969.

/36/ R.L.D. Chane, K.G.T. Hollands, G.D. Raithby, T.E. Unny:
Free Convection Heat Transfer Across Inclined Honeycomb Panels;
J. Heat Transfer, 86-91, Febr. 1977.

/37/ M. Dubois, P. Bergé:
Experimental Study of the Velocity Field in Rayleigh-Bénard-Convection;
J. Fluid Mech. 85, 641-653, 1978.

/38/ J. Wesfreid, Y. Pomean, M. Dubois, C. Normand, P. Bergé:
Critical Effects in Rayleigh-Bénard Convection;
Le Journal de Physique 39, 725, 1978.

/39/ J. Wesfreid, P. Bergé, M. Dubois:
Induced Pretansitional Rayleigh-Bénard Convection;
to be published in Phys. Letters A (private Communication).

/40/ C.R. Hoard, C.R. Robertson, A. Acrivos:
Experiments on the Cellular Structure in Bénard Convection;
Int. J. Heat Mass Transfer 13, 849-856, 1970.

/41/ G. Ahlers:
The Rayleigh-Bénard Instability at Helium Temperatures in Fluctuations Instabilities and Phase Transition;
Ed. Riste, Plenum Press, 1975.

/42/ J. Tavantzis, E.L. Reiss, B.J. Matkowsky:
On Smooth Transition to Convection;
SIAM J. Appl. Math. 34, 322, 1978.

/43/ P.G. Daniels:
The Effect of Distant Side Walls on the Transition to Finite Amplitude Bénard Convection;
Proc. Roy. Soc. Lond. A.358, 173-197, 1977.

/44/ P. Hall, I.C. Walton:
The Smooth Transition ot a Convective Regime in a Two-Dimensional Box;
Proc. Roy. Soc. Lond. A358, 199-221, 1977.

/45/ S.N. Brown, R. Stewartson:
On Thermal Convection in a Large Box;
Stud. Appl. Math., 57, 187-204, 1977.

/46/ S.N. Brown, K. Stewartson:
On Finite Amplitude Bénard Convection in a Cylindrical Container;
Proc. Roy. Soc. Lond. A360, 455-469, 1978.

/47/ P. Hall, I.C. Walton:
Bénard Convection in a Finite Box: Secondary and Imperfect Bifurcation;
J. Fluid Mech. 90, 377-395, 1979.

/48/ E.L. Tarunin:
Convection in a Closed Cavity Heated from Below when Equilibrium Conditions are Disturbed;
Fluid Dynamics 12, 340-345, 1977.

/49/ R. Krishnamurti:
On the Transition to Turbulence Convection, Part 1: The Transition from Two to Three-Dimensional Flow;
J. Fluid Mech. 42, 295-307, 1970.

/50/ E.L. Koschmieder:
On the Wave Length of Convective Motions;
J. Fluid Mech. 35, 527-530, 1969.

/51/ E.L. Koschmieder:
Bênard Convection;
Advances in Chemical Physics, 26, 1973.

/52/ J.A. Whitehead, jr.:
A. Survey of Hydrodynamic Instabilities, in Fluctuations
Instabilities and Phase Transitions;
Ed. Riste Plenum Press, 1975.

/53/ P. Bergé:
Experiments on Hydrodynamic Instabilities and Transition
to Turbulence, Dynamic Critical Phenomena and Related Topics;
Lecture Notes Physics 104, Springer 1979.

/54/ H. Oertel:
Thermische Zellularkonvektion;
Habilitationsschrift Universität Karlsruhe, 1979.

/55/ J. Maurer, A. Libchaber:
Rayleigh-Benard Experiment in Liquid Helium Frequency
Locking and onset of Turbulence;
Le Journal de Physique 40, 419-423, 1979.

/56/ J.N. Koster:
Freie Konvektion in vertikalen Spalten;
Dissertation Universität Karlsruhe, 1980, KfK-Bericht 3066.

/57/ J.M. Olson, F. Rosenberger:
Convective Instabilities in a Closed Vertical Cylinder
Heated from Below, Pt. 1: Monocomponent Gases;
J. Fluid Mech. 92, 609-629, 1979.

/58/ I.A. Azouni, C. Normand:
Thermoconvective Instability of Water Between 0^{o} and 4o
;
To be published in J. Fluid Mech., 1981.

/59/ P. Gollub, S.V. Benson:
Many Routes to Turbulent Convection;
J. Fluid Mech. 100, 449-470, 1980.

/60/ G. Ahlers:
Low Temperature Studies of the Rayleigh-Bénard Instability and Turbulence;
Phys. Review Letters 33, 1185-1188, 1974.

/61/ G. Ahlers, R.P. Behringer:
Evaluation of Turbulence from the Rayleigh-Bénard Instability;
Phys. Rev. Letters 40, No. 11, 712-716, 1978.

/62/ J.P. Caltagirone:
Thermoconvective Instabilities in a Horizontal Porous Layer;
J. Fluid Mech. 72, 269-287, 1975.

/63/ D.V. Lyubimov, G.F. Putin, V.J. Chenatynskii:
On Convective Motions in a Hele Shaw Cell;
Sov. Phys. Dokl. 22(7), 1977.

/64/ G.F. Putin, E.A. Tkacheva:
Experimental Investigations of Supercritical Convective Motions in a Hele Shaw Cell;
Fluid Dynamics 14, 1-5, 1979.

/65/ L. N. Howard:
Convection at High Rayleigh Number;
Proc. 11th Int. Congr. on Appl. Mech; München, H. Gortler ed., Springer Berlin 1964, 1109-1115.

/66/ P. Bergé, M. Dubois:
Different Routes to Turbulence in High Prandtl Number Convection and in Rectangular Cells: Influence of Aspect Ratio and of Structure;
in: Systems far from Equilibrium; Lecture Notes in Physics 132, 1980.

/67/ A. Libchaber, J. Maurer:
Local Probe in a Rayleigh-Bénard Experiment in Liquid Helium;
Journal de Physique, Letters L369, 1978.

/68/ H. Frick:
Zellularkonvektion in Fluidschichten mit zwei festen seitlichen Berandungen;
Dissertation Universität Karlsruhe, 1980, KfK-Bericht 3109.

/69/ O. Kvernvold:
On the Stability of Non-Linear Convection in a Hele-Shaw Cell;
Int. J. Heat Mass Transf. 22, 395-400, 1979.

/70/ J.W. Elder:
Physical Processes in Geothermal Areas;
in: 'Terrestrical Heat Flow' Chapt. 8, Ed. W.H.K. Lee, Amer. Geophys. U. Monograph, No. 8.

/71/ M. Dubois, P. Bergé:
Experimental Evidence for the Oscillators in a Convective Biperiodic Regime;
Phys. Lett. 76A, 53-56, 1980

/72/ Cl. Günther;
Numerische Untersuchungen der Naturkonvektion in einer von unten beheizten, schmalen Hele-Shaw Zelle;
KfK 3142, Kernforschungszentrum Karlsruhe, 1981.

/73/ J.W. Elder:
Convection in a Porous Medium;
J. Fluid Mech 27, 609-623, 1967.

/74/ J.W. Elder:
The Unstable Thermal Interface;
J. Fluid Mech. 32, 69-96, 1968.

/75/ S. Bories:
Sur les mécanismes fondamentaux de la convection naturelle en milieu poreux;
R.G.T. 108, 1377-1401, 1970.

/76/ J.P. Caltagirone, M. Cloupeau, M. Combarnous:
Comptes Rendus 273, 833-836, 1971.

/77/ R.A. Horne, M.J. O'Sullivan:
Oscillatory Convection in a Porous Medium Heated from Below;
J. Fluid Mech. 66, 339-352, 1974.

/78/ R.A. Wooding:
Instability of a Viscous Liquid of Variable Density in a Vertical Hele-Shaw Cell;
J. Fluid Mech. 7, 501-515 1960.

/79/ J. Bear:
Dynamics of Fluids in Porous Media;
American Elsevier, Publishing Company 1972.

/80/ B.K. Hartline, C.R.B. Lister:
Thermal Convection in a Hele Shaw Cell;
J. Fluid Mech. 79, 379-391, 1977.

/81/ E.M. Sparrow, R.J. Goldstein, V.K. Jonsson:
Thermal Instability in a Horizontal Fluid Layer; Effect of Boundary Conditions and Non-Linear Temperature Profile;
J. Fluid Mech. 18, 513-528, 1964.

/82/ S.H. Davis:
The Stability of Time-Periodic Flow;
Annular Review of Fluid Mech. 8, 57-74, 1976.

/83/ S.H. Davis, S. Rosenblat:
On Bifurcating Periodic Solutions at Low Frequency;
Studies in Applied Mathematics 57, 59-76, 1977.

/84/ N. Minorsky:
Nonlinear Oscillations;
Van. Nostrand, 1962.

/85/ J.A. Whitehead:
A Survey of Hydrodynamic Instabilities in Fluctuations,
Instabilities and Phase Transition;
Ed. Tormod Riste, Plenum Press, 1975.

/86/ J. Catton:
Convection in a Closed Rectangular Region; The Onset of Motion;
J. Heat Transfer, 186-187, Febr. 1970.

/87/ R.N. Horne, J. P. Caltagirone:
On the Evolution of Thermal Disturbances During Natural
Convection in a Porous Medium;
J. Fluid Mech. 100, 385-395, 1980.